Bull. Spec. Astrophys. Obs., 2003, 56, 57-90

The multifrequency monitoring of microquasars. SS433

S. A. Trushkin, N. N. Bursov, N. A. Nizhelskij

Special Astrophysical Observatory of the Russian AS, Nizhnij Arkhyz 369167, Russia

Received December 19, 2003; accepted December 24, 2003.

Abstract. The principal results of daily observations with the RATAN-600 radio telescope of X-ray binary with relativistic jets microquasar SS433 in 1986–2003 are presented. We have measured the flux densities at 0.96, 2.3, 3.9, 7.7, 11.2 and 21.7 GHz in different sets, duration from a week to some months. In general there are 940 observations of SS433 and more than 4500 flux density measurements in the period. Observations show that radio spectra are well fitting by a power law. The mean spectral index remained the same, -0.60 ± 0.14 during almost 20 years at least, and mean accuracy of the index determination was better than 0.1 in our multi-frequency observations, i.e. it was higher than in the intensive two-frequency monitoring of SS433 with the three-element GBI interferometer. Flux density data and spectra 'on-line' plotting are accessible on the CATS data base site: http://cats.sao.ru/.

Key words: X-rays: binaries – stars: flare – stars: individual: SS433 – jets – radio continuum: stars – monitoring

1. Introduction

The X-ray binaries (XBs) have long been studied in radio band. After an identification of Cyg X-3 in the beginning of the 70-s it became evident that XBs could have powerful variable radio emission. A sample of X-ray binaries with relativistic jets that Mirabel & Rodriguez (1999) named microquasars consists of 15–20 objects. The brightest of them were observed actively under a monitoring program of XBs with the RATAN-600 radio telescope (Trushkin 2000, Trushkin & Bursov 2001).

SS433 — a bright variable emission star — was identified by Clark and Murdin (1978) with a rather bright compact radio source 1909+048 located in the center of a supernova remnant W50. When in 1979 mobile optical emission lines were discovered in the spectrum of this bright star SS433 — a radio source 1909+04 (Margon et al. 1979), it became apparent that a new class of objects in the Galaxy was found. At the same time Spencer (1979) was the first to discover an extended structure: a compact core and 1 arcsec long aligned jets in the radio image of SS433. At present such a structure in microquasars is commonly named a radio jet. Different data do indicate a presence of a very narrow (about 1°) collimated beam at least in X-ray and optical ranges. At present there is no doubt that SS433 is related to W50. SS433 is probably a stellar remnant of a SN that exploded in a binary system about 30000 years ago. An explosion of one of the components did not destroy the binary. A distance to SS433 of 4.8 kpc was later determined by different ways including the direct measurement of proper motions of the jet radio components.

As is now known, this unique variable X-ray, IR and radio source is an eclipsing binary cosisting of a compact object and an early type massive star. The system has a pair of opposite relativistic (in which matter is ejected at 0.26c) jets, which show themselves in different ways in different ranges from X-ray to radio. The VLBI (Very Long Baseline Radio Interferometry) observations of the jets proper motion showed that they consist of separate blobs that move ballistically at the same velocity 0.26c. Resultant from the 164-day precession of a thick accreting disk the jets rotate along conic surface and look like structures similar to a twin corkscrew on VLA radio maps (Hjellming & Johnston 1981).

There are strong evidences for believing that this binary system consists of a relativistic star with an accreting disk and a massive optical component filling its Roche lobe. The supercritical accretion onto the relativistic star is likely to lead to initiation of the SS433 main feature — two opposite jets of matter moving from the accretion disk poles at a velocity of about a quarter of the speed of light. The recent intensive spectral investigation made it possible to determine rather precisely the SS433 mass function and to estimate the relativistic component mass. It is equal to 11 ± 5 $M_\odot$ (Gies et al. 2002a,b) what suggests that this is a black hole. Absorption lines in the SS433 spectrum belonging to the optical component are almost identical with those in the spectrum of an

evolved star of a mid-A spectral class with a mass of 19 ± 7 $M_\odot$.

These jets that had been first discovered in spectral optical observations are seen also in X-ray and radio wavelengths. Activity phenomena in SS433 give rise to strong variability of all its electromagnetic spectrum.

As is seen from the jet X-ray images and from an oblong form of the radio remnant W50, the jet structure extends up to size scales of 1°. It gives an estimate of jets age as $\sim$ 1000 years. A simple kinematic model of SS433 (Abell & Margon 1979) with collimated jets was verified as a whole by many observational data (Margon 1984).

SS433 is still the unique object in the Galaxy, in which the relativistic opposing jets appear in Doppler-shifted optical and X-ray emissions, i.e. beside the relativistic radio-emitting electron-positron plasma a baryonic matter with high atomic numbers moves in the SS433 jets (Kotani et al. 1996, Marshall et al. 2002).

The major contribution to the study of temporal and spectral properties of microquasars was made by long-term program of variable sources monitoring at two frequencies of 2.25 and 8.3 GHz with GBI (Green-Bank Interferometer, NRAO). The publicly available data totally include about 16000 measurements of flux density of SS433. Fig.1 shows the light curve of SS433 in 1979–2000 which cover all its GBI-observations at a frequency of 2.25 GHz. The results of these studies were partly published by Johnston et al. (1984) and Fiedler et al. (1987).

From recent interesting results of the SS433 study noteworthy is the circular polarization of its emission in cm range detected by Fender et al. (2000) and a sign change of the Stokes parameter V detected by McCormick et al. (2003) in the 1–9 GHz range. It might be related either to the presence of a gyro-synchrotron radiation emitted by relatively low-energy electrons or to the change in a configuration of collimated magnetic field in the jets.

Space observatory INTEGRAL first registered a variable hard X-ray emission (25–100 keV) (Cherepashchuk et al. 2003). It was shown that the emission level is influenced by the precession and orbital motions. These observations in high energy range confirm indirectly once more a presence of a black hole in this XB.

In radio band a quasisteady synchrotron emission of SS433 with spectrum $S_\nu \sim S_0\nu^\alpha$ is superimposed by a non-thermal flares, when the flux density can exceed the quiescent level 10 times. The SS433 radio flares are not rare, although the periods of relative quiescence can be as long as 100–200 days.

At the flares onset there are evidences of synchrotron source opacity (a flat spectrum) and with further gradual decay of the flare the spectrum becomes steeper. The maximum flux of a flare comes later at lower frequencies as was shown for SS433 by Fiedler et al. (1987), Vermeulen et al. (1993a,b), Bursov & Trushkin (1995); for Cyg X-3 see Waltman et al. (1994, 1995, 1996) and for GRS 1915+105 — Trushkin et al. (2001) and Fender et al. (2002). It corresponds to evolution of an adiabatically expanding cloud of relativistic emitting electrons. Shklovskij (1960) and van der Laan (1966) were the first to formulate basic equations describing this evolution.

Different modifications of this model necessary for observations fitting include a hollow conic geometry of jets, an account for synchrotron losses or reverse Compton scattering, a dynamic motion outwards a thermally absorbing envelope. Computations of flares based on a model of twin conic jet show a remarkable coincidence with observations for Cir X-1 (Garcia 1995), SS433 (Hjellming & Johnston 1988), LSI+61° 303 (Paredes et al. 1991), Cyg X-3 (Marscher at al. 1975, Marti et al. 1992) and SAXJ1819-254 (Hjellming et al. 2000).

Based on data of ten SS433 flares in 1986–87, Trushkin (1989) showed that on average they have close frequency power relations for the maximum flare flux and the time of this maximum occurrence:

$$\Delta S_m(\mathrm{Jy}) = 1.3\nu^{-0.4\pm0.15},$$

$$\Delta t_m(\mathrm{days}) = 5\nu^{-0.4\pm0.1},$$

where ν is in GHz.

A gradual flare decay follows one of two time laws. An original model of Shklovskij – van der Laan provides the power law. In many microquasars there was actually detected the radio emission decay according to the law

$$S_\nu = S_o\, t^{-2p}\nu^\alpha,$$

where $p \approx 2$ is an index of a power electron distribution that is related to the spectral index

$$\alpha = (1-p)/2 \approx -0.5$$

for an optically thin source. It is in excellent agreement with a possible diffusive mechanism of relativistic electrons acceleration in shock waves. At a compression index in a strong shock wave $\rho \leq 4$ the spectral index of these electrons is

$$p = (\rho+2)/(\rho-1) = 2.$$

Other flares and fluxes of plasmons in jets were decaying according to the exponential law

$$S_\nu = S_0 e^{-t/\tau}$$

(for SS433 see Jowett & Spencer 1995). A diminution of the characteristic time τ with frequency was often but not always observed. A relation

$$\tau(\mathrm{days}) = 11.5\ \nu^{-0.29\pm0.03}$$

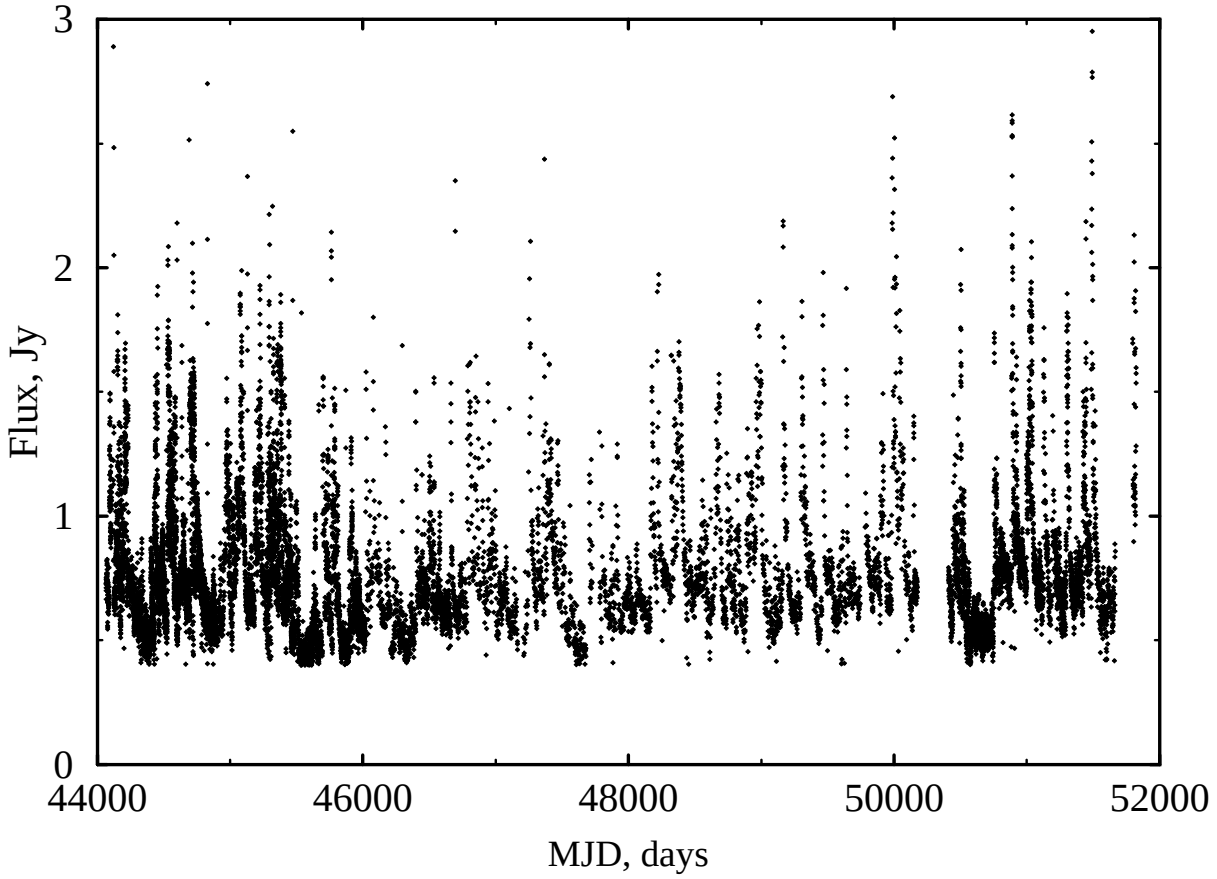

Figure 1: *The SS433 light curves at a frequency of 2.25 GHz by data of GBI (NRAO/NASA).*

Table 1: *A flux density sensitivity of the "Northern Sector" of RATAN-600*

Wavelength (cm)	31.2	13.0	7.6	6.2	3.9	2.7	1.38
Frequency (GHz)	0.96	2.3	3.9	4.9	7.7	11.2	21.7
ΔS(mJy)	40	15	3	3	8	10	20

where ν is in GHz was observed in Cyg X-3 (Trushkin 1998). In Cyg X-3 a transit from the exponential law to the power one was detected several times (Hjellming et al. 1974, Marscher et al. 1975, Bursov & Trushkin 1995, Trushkin 1998) what is interpreted as a transit from a mode with a dominated radiative losses to a mode of adiabatic expansion.

Spencer (1996) calculated the energy of the jet components based on the condition for minimum energy of relativistic particles and of magnetic field what is fulfilled at an equipartition of energy of these components. He showed that a considerable not to say prevailing part of energy released during flares belonged to radio emitting particles and magnetic field of jets.

Below we discuss a few large monitoring programs carried out at the Northern Sector of RATAN-600 having resulted in the SS433 light curves at 4–6 frequencies.

2. Observations and processing

A part of observations was carried out in the program of the studies of variable X-ray sources in long-term cycles of the monitoring of flare activity (Trushkin 2000, Trushkin et al. 2001a,b). A regular complex of continuum spectrum radiometers was used. The receivers of frequencies 3.9, 7.7, 11.2 and 21.7 GHz were equipped with cryogenic systems of closed loop that depress the temperature of the first amplifier stages down to 15–20 K. The radiometers of frequencies 0.96 and 2.3 GHz were equipped with low-noise transistor amplifiers. Besides, to avoid the narrow-band interference from mobile communications and locators, the wide bands of these receivers were cut into 4 and 8 subchannels correspondingly. It should be mentioned

that from the midyear 2002 there have been no observations at 960 MHz because of a powerful interference generated by cellular transmitters in a range of 910 MHz mounted near the RATAN-600.

The observation was fulfilled by the RATAN-600 Northern Sector or Southern Sector plus a Flat reflector every day at the source culmination, i.e. the UT time of observations was changing during every cycle, whereas the local sidereal time of observation was remaining the same. In an observation the flux from a source was recorded at two–six frequency ranges. In spite of a bright galactic background the telescope angular resolution is sufficient to detect reliably SS443 on drift scans.

Table 1 lists observational sensitivities of the telescope RATAN-600 (a level 1σ at the optimal smoothing of records) in a single transit of the source through a fixed beam pattern. Unfortunately, because of frequent interferences the pointed sensitivity was not always achieved in real observations. Generally the antenna of the Southern Sector with the Flat reflector had a noticeably lower system flux sensitivity because of higher antenna noise temperature and smaller effective area in comparison to the antenna of the Northern Sector.

On November 6, 2003, the receiver at frequency 3.9 GHz was replaced by a new high sensitive cryogenic two-channel radiometer at frequency 4.9 GHz.

Every day during all cycles the calibration sources 1345+12, 1850-01 or 2128+04 were observed. Their current fluxes were calibrated using the secondary calibration sources: 3C286, NGC7027, DR21 and some others. We suggest that the SS433 flux measurement error does not exceed 3–8% at all frequencies: 0.96, 2.3, 3.9, 11.2 and 21.7 GHz.

The fluxes for secondary calibration sources were taken from a paper by Aliakberov et al. (1985), which in turn were in the basic radio-astronomical flux scale of reference sources by Baars et al. (1977) and with updated flux measurements in a paper by Ott et al. (1994). The fluxes of reference sources accepted for the present measurement cycle are given in Table 2.

The digital recording of data, preliminary processing and archiving were made by the acquisition software packages created by P. Tsybulev and V.K. Kononov. The processing of obtained records of target and reference sources was made with a data-processing program "*prat*". Data processing included the procedures of background and pulse interferences removal, the convolution with the beam pattern, and the Gauss analysis.

2.1. Study of SS433 in the experiment "Cold"

Undertaken in 1980 a 100-day observational set on searching for microwave background fluctuations was carried out at a fixed antenna angle of elevation 51° (i.e. at a declination chosen to observe every day SS433 Dec1950 = +04°57′) with an unmoved feed-cabin (Parijskij & Korol'kov 1986). This mode is the most optimal to study the fast flux variability of radio sources. Thus, dozens of instantaneous SS433 spectra in the range from 3.9 to 31 cm were obtained in daily observations. In February–May 1980 SS433 did not show strong variability. The absence of bright flares allowed carrying out the Fourier analysis of the SS433 radio brightness with the purpose of searching for radio flux periodicity reflecting intrinsic binary periodicities: 13-day orbital period or its half of 6.5 days.

A low detectable harmonic of 6.5 ± 0.5 days appeared in a sample of the cycle onset in February–March 1980, but later it was not detected. In the 13-day-average observations at a wavelength of 2.08 cm there is also a detectable harmonic of the 13-day period, but the data were not sufficient for final conclusion about the existence of periodicity in the quiescent radio emission of SS433.

Only on basis of many observations in 1997 and 1999 and due to a precise calibration by the flux density we managed to unambiguously detect a 6.05-day modulation of the quiescent radio emission of SS433 at all the six frequencies (Trushkin et al. 2001).

A faint flare that is seen the best at 8.2 cm wavelength correlates with variations of the photometric flux (Gladyshev 1981). In Fig.2 a typical delay of the radio flare relative to the optical one and the general similarity of light curves are clearly seen. Neizvestnyj et al. (1980) also made a conclusion about the delay of radio flares. In observations of 1980 a substantial linear polarization of SS433 radiation at a level of 5–10% was first detected. Hjellming and Johnston (1981) showed that the high linear polarization is related to jet ejections, whereas the central core ($< 0.1''$) is not polarized. On the average, the SS433 flux in the centimeter range in the quiescent state of this cycle is fitted well by the formula

$$S_\nu(\mathrm{Jy}) = 1.1\nu^{-0.6}(\mathrm{GHz}).$$

There are near 300 other observations of SS433 during other "Cold" sets from 1988 to 1994 that are not included in the paper.

2.2. General behaviour of the SS433 radio emission

We list all measurements carried out with the radio telescope RATAN-600 from December 1986 to January 2004 in Table 3. The first column of the table gives a modified Julian date of observation MJD = JD-2400000.5, columns 5–8 give flux densities (in mJy) at frequencies of 0.96, 2.3, 3.9, 7.7, 11.2 and 21.7 GHz. Note that from November 6 of 2003 the receiver at 3.9 GHz was replaced with a two-channel cryo-radiometer at a frequency of 4.9 GHz.

Table 2: *Flux densities of reference sources (Jy)*

Name	Another	Frequency (GHz)						
of source	name	0.96	2.3	3.9	4.9	7.7	11.2	21.7
1328+30	3C 286	17.2	11.5	8.55	6.45	5.52	4.25	2.5
1345+12		6.48	4.4	3.31	2.55	2.21	1.74	1.12
1850-01	HII		2.27	3.06	3.63	3.88	4.19	4.49
2037+42	DR 21	5.0	12.1	17.4	19.9	21.7	21.7	20.7
2105+42	NGC 7027	0.9	2.64	4.9	5.54	6.33	6.03	5.9

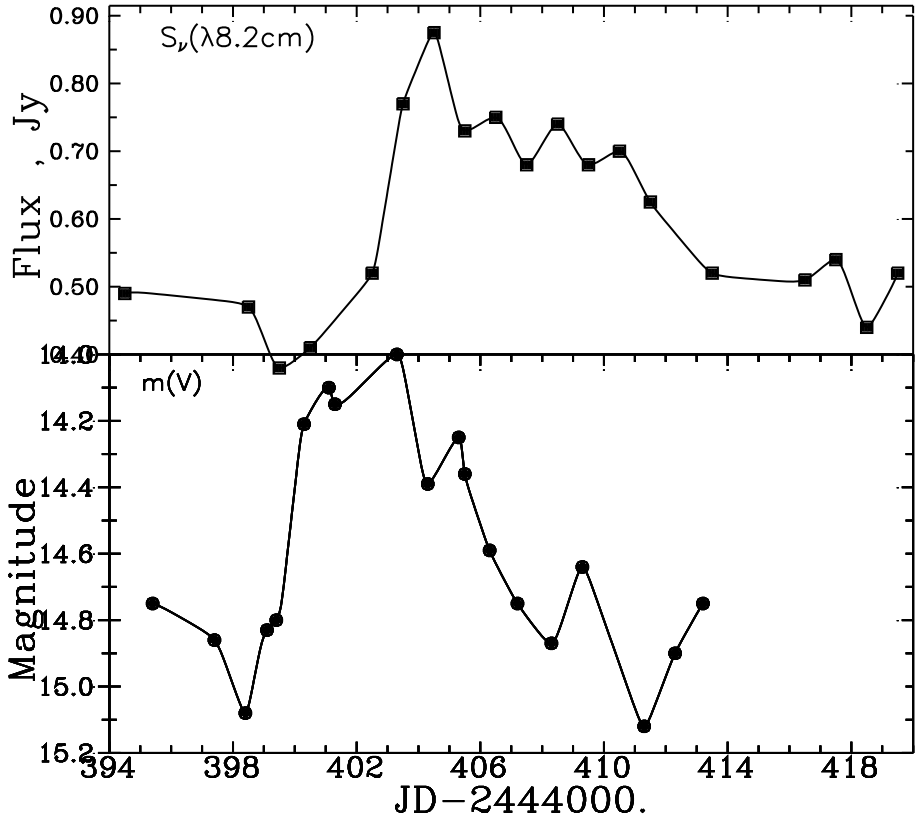

Figure 2: *The SS433 light curve in V band and the curve of flux variations at 8.2 cm wavelength in June 1980.*

The absence of some numbers from these columns means that either there was no observation or it failed because of one or another reason (atmospheric or electric interferences, a radiometer trouble, etc.). Column 9 gives the calendar date of observation (ddmmyy) and in columns 10 and 11 a spectral index and its error are given, they are determined from a fitting of a 2–6-point spectrum by a single power law: $S_\nu = S_o\nu^\alpha$. Summarily there were 940 observations of SS433, and 4500 flux densities were measured.

The data of the flux density measurements are publicly-accessible as a web-program for plotting the SS433 spectra 'on-line' on the web-server of the CATS data base (Verkhodanov et al. 1997): http://cats.sao.ru/cgi-bin/ss433.cgi. To get the spectrum plots and fitting parameters directly on the monitor screen a user is only to choose a modified Julian (MJD) or calendar date of the SS433 observation.

Fig.3 shows a histogram of spectral index distribution by total data from Table 3. The daily spectra were well fitted by a power law relation, a mean spectral index remained the same, -0.60 ± 0.14 over 20 years, and the spectral index determination error (column 11 in the table) of our measurements being better than 0.1 on the average. It is intriguing that in the centimeter wavelength band the spectrum of SS433 is always optically thin with the spectral index α varying from -0.2 to -1.4, i.e. there is no case with a positive index or inverse spectrum. However, a reservation should be made: we are dealing with an integral spectrum of SS433; if we subtract

a "quasi-constant" component of the flux, then the flares spectra can be inversion ones evidently because of the delay of flares at low frequencies. The mean flux for ~ 600 measurements at a frequency of 960 MHz is equal to 1530 mJy.

It should be noted that in our observations the spectral index measurement accuracy is higher than that in a two-frequency program of SS433 monitoring with the three-element radio interferometer GBI in Green-Bank (USA). From publicly-accessible data of GBI one can estimate an average spectral index to be -0.70 ± 0.30 by 15000 measurements at frequencies of 2.25 and 8.3 GHz. As was shown by the analysis of measurements fulfilled in the same time, this significant difference in the average spectral index is due to the fact that GBI fluxes at 8.3 GHz are underestimated by 10–15 %, though "our" 2.3-GHz fluxes and GBI 2.25-GHz fluxes practically coincide, what resulted in a steeper average spectrum of SS433 by GBI data in comparison with what was obtained by our data. One can assume that the cause of a lower measured flux at the high frequency is a partial resolution of SS433 by the GBI interferometer with the base of 2.4 km.

2.3. Search for regularities in the radio flares of SS433

In December 1986 – March 1987 a long-term cycle of observations of SS433 radio flares was carried out. Six rather powerful flares were detected at wavelengths of 3.9, 7.6, 13 and 31.2 cm during this 90-day cycle. Fig.5 shows light curves at these frequencies.

During 2–3 weeks of May 1987 an international multi-wave monitoring campaign was carried out on SS433 (Vermeulen et al. 1993a,b), when this object was observed in coordination with several radio telescopes (MOST, VLA, NRAO GBI, RATAN-600, Bologna Cross and European VLBI) and many optical telescopes.

In Fig.6 we present the curves of flux variability (S_{tot} – S_q) during 19–31 May 1987. It is seen that in this period we managed to record two powerful flares, the second one being apparently related to the increase of flux in a separate component (a blob) of the jet in a so-called zone of "brightening" (Vermeulen et al. 1993a). The recent active mapping of SS433 with an interferometer of the highest resolution VLBA (NRAO, USA) undertaken in Summer 2003 during 42 days (Mioduszevski et al. 2003) have shown that the blobs do not all necessarily become brighter on the 5^{th}–6^{th} day of the travel from a center (50 mas) what has been shown by Vermeulen et al. (1993b). Such brightening can occur earlier or not occur at all, and the brightening phenomenon can be related to selected azimuths of jets. Sometimes the blobs brightening can be very strong, up to 30 times and occur at equal distances/times from XBs (subject to relativistic effects). The motion conditions of separate blobs change depending on the activity of so-called "anomalous" outflows across jets or near the plane of accreting disk of this XB. The velocity of these motions (~ 10000 km/sec), which was measured in this set for the first time, is so high that it necessarily impacts a lot the filling of a channel generated by the motion of jets along the 164-day precession trajectory. Interestingly, the motions at velocities of 0.1–0.15 c in the radio structures of SS433 were also detected earlier (Stirling et al. 2002).

In Fig.4 we present the radio emission light curves of SS433 during a long-term observational set of duration almost one and a half year in 2002–2004. A rather quite period during a year was broken by a relatively powerful flare only in the end.

Here we should touch on a very interesting phenomenon — a pre-flare flux fall below an average quiescence level at all frequencies. The "negative" fluxes in Fig.6 are caused by such a "dip". Such short ($\sim 1-2$ days) dips were observed in SS433 more than once, although not before all flares. The dips of the quiescent emission are estimated as $\sim 100-200$ mJy.

At least three such dips of the SS433 radio emission before the flares in MJD52213, 52325 and 52274 are seen in Fig.5. It is interesting that between the first and the second flares the observations with the satellite RXTE in a range of 2–12 keV were fulfilled and in a number of measurements the detection of strong X-ray flux variability has been gained in an interval about 3000 seconds (Kotani et al. 2002). In Fig.4 the dip of SS433 radio emission before the flare in the interval MJD52985–52995 is well noticeable.

Perhaps, the dips are related to the appearance of optically thick matter, that resulted from heavy accretion prior to powerful flares (Waltman et al. 1994). Then either optical depth of this matter decreased because of fast expansion or a plasmon, which is responsible for the flare, "resurfaces" from this absorbing matter and deletes the flux deficit. Since the dip concerns the quiescent component of the SS433 flux, all environment of the binary system as well as jet insides are supposedly rearranged.

The phenomenon of dip was observed only before the first flare after a long quiescent period, but it is not improbable that we cannot see it before all flares because of an overlap of flares. For example, in the flare of May–June 1996 (Fig.9) there are no visible flux fall-down at all frequencies.

Finally, it is noteworthy that an analogous effect is pronounced more strongly in another microquasar Cyg X-3, where the flux dip duration correlates with the power of subsequent flare and the lowest (at the detection threshold) level of hard X-ray flux (Trushkin 1998).

Using all SS433 observations carried out with

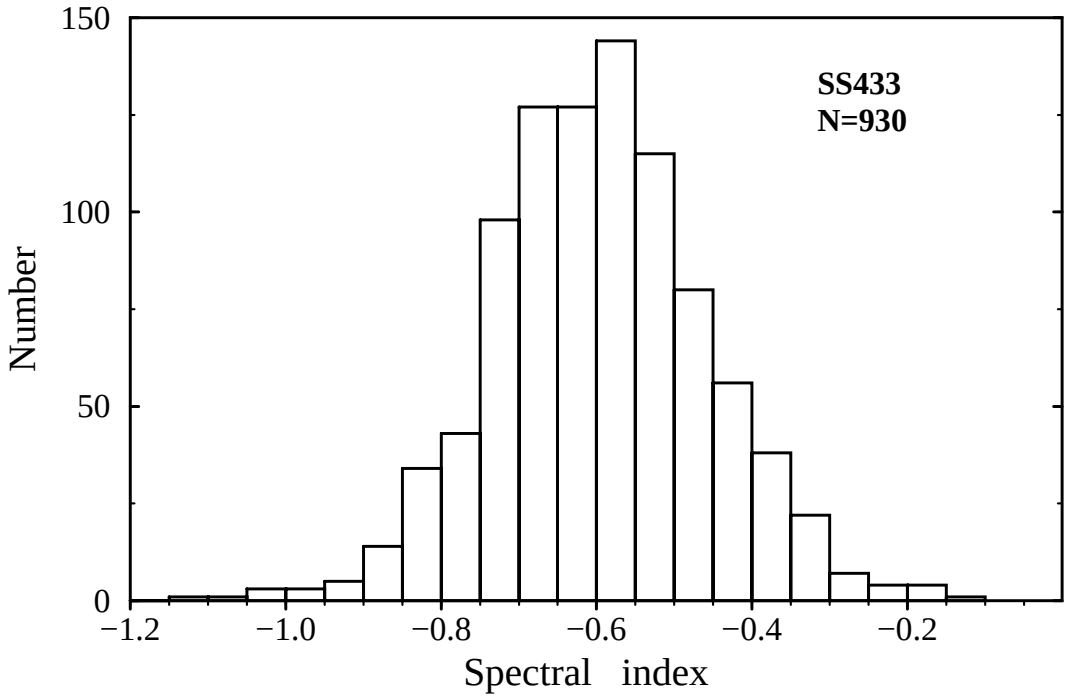

Figure 3: *The bar chart of the SS433 spectral index distribution by 930 measurements wih RATAN-600.*

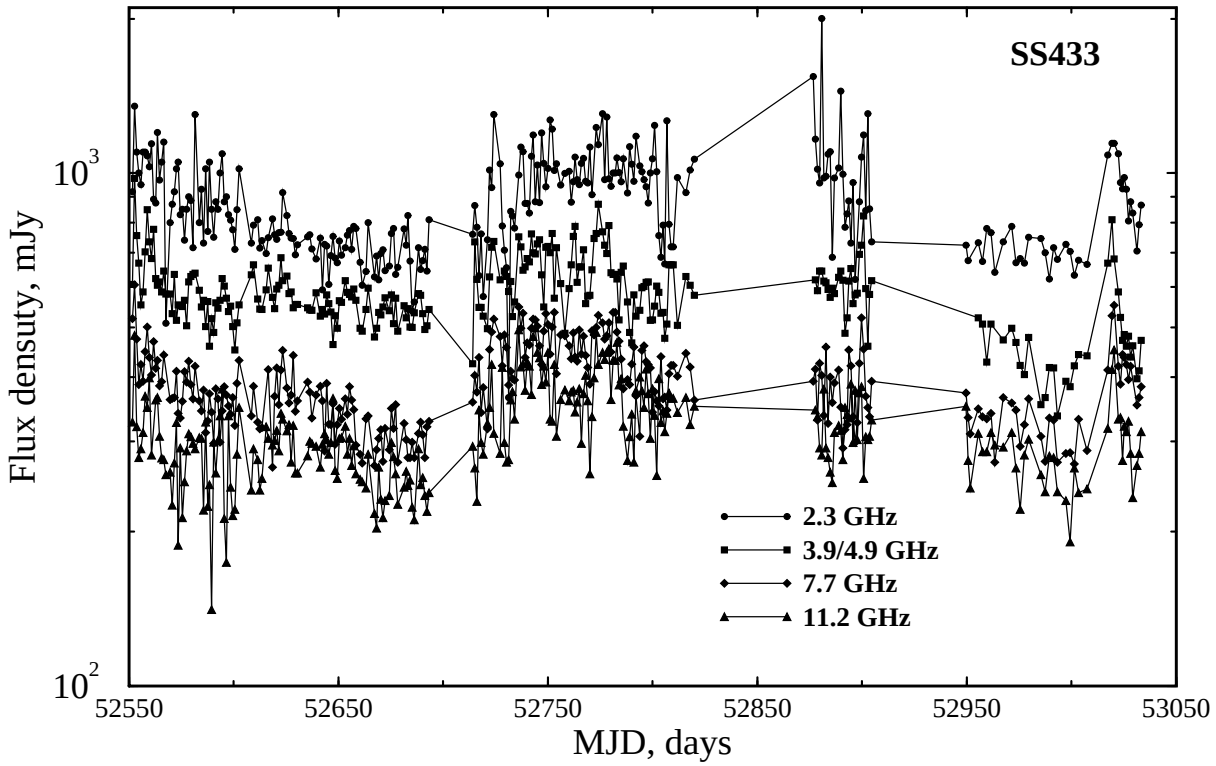

Figure 4: *The long-term period of SS433 observation with RATAN-600 from October 2002 to January 2004.*

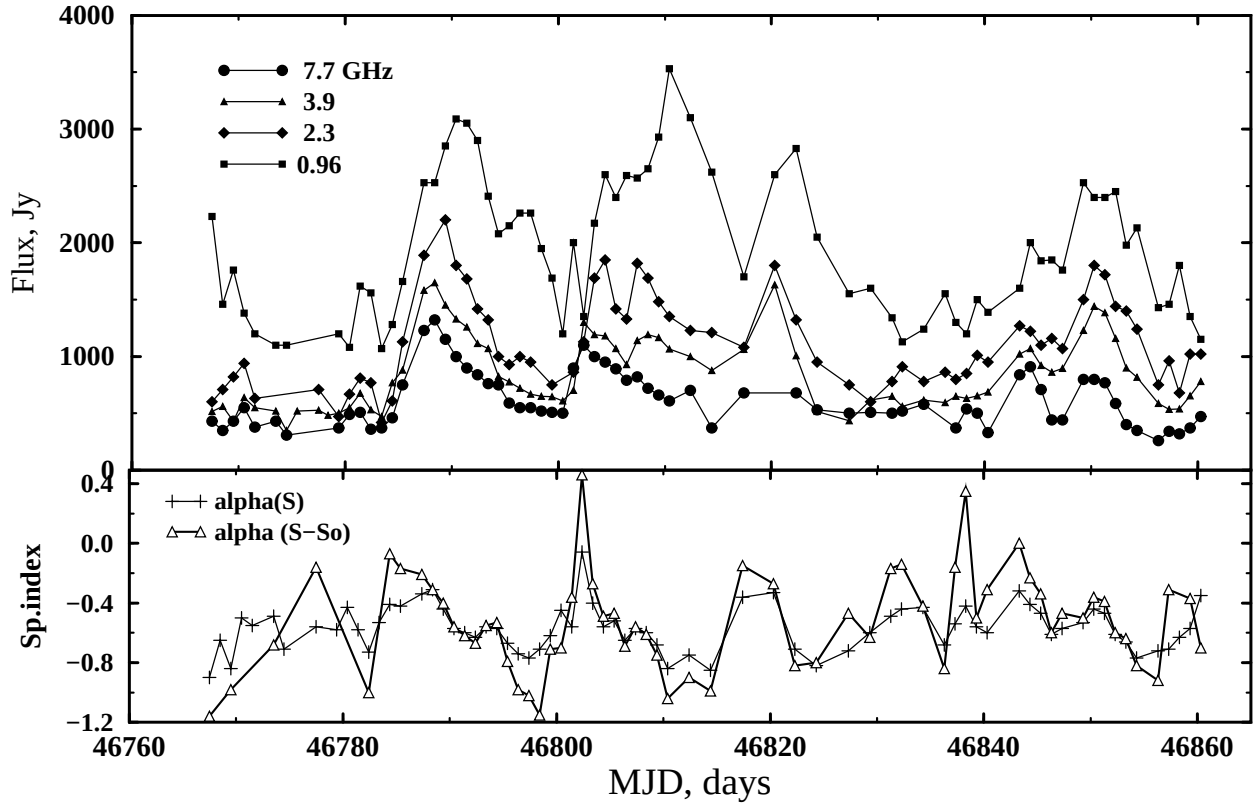

Figure 5: *The radio emission light curves of SS433 at wavelengths 3.9, 7.6, 8.2, 13 and 31 cm in December 1986 – March 1987 and variations of the spectral index of the total radio emission and that after subtraction of the quiescent flux levels.*

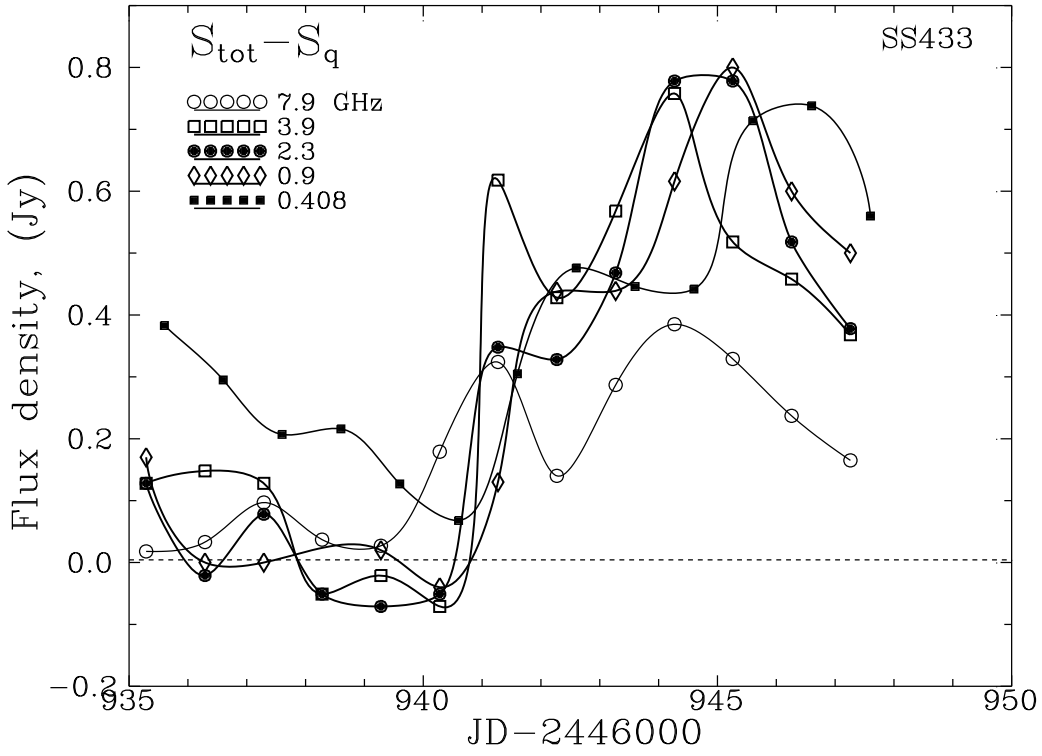

Figure 6: *The radio emission light curve of SS433 at different frequencies in May 1987. The constant part of flux (S_ν = 1.1 $\nu^{-0.58}$) was removed. The data at 843 and 960 MHz and at 7700 and 8085 MHz were averaged.*

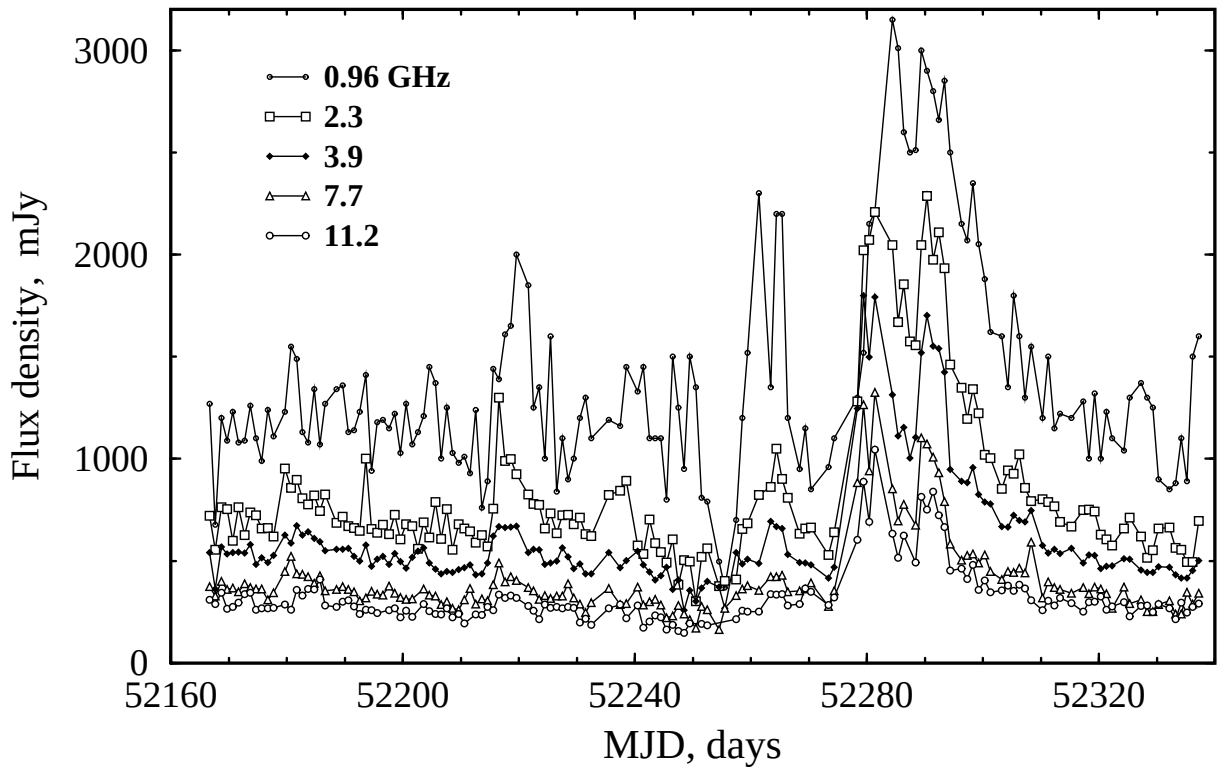

Figure 7: *Long-term observations of SS433 with RATAN-600 from September 2002 till March 2003.*

RATAN-600 including reprocessed observations from a paper by Neizvestnyj et al. (1980) we obtained average characteristics of radio flares.

The flares last 3–15 days, the flux density variation can reach 0.5–0.8 Jy at a frequency of 7.7 GHz and 2–3 Jy at 960 MHz. The main flare parameters were analyzed: the dependence of the flare maximal flux ΔS_m and its time Δt_m on frequency. It turned out that these relations are well fitted by power laws with indices indicated for each flare. Average over 9 flares parameters of these relations are below.

$$\Delta t_m = \Delta\, t\cdot\nu^m,\ m = -(0.20-1.0),\ \overline{\Delta t_m} = 5.1\cdot\nu^{-0.43}$$

$$\Delta S_\nu = \Delta\, S\cdot\nu^n, n = -(0.15-0.9),\ \overline{\Delta S_\nu} = 1.3\cdot\nu^{-0.46},$$

where in the last formulae the flux is in Jy and the frequency is in GHz.

What the above relations are valid during long period of time is the most important property of radio flare. The flare increase is always steeper than its fading that indicates a different size of emission region at flare onset and end. Fig.8 shows how reliably the power law for Δt_m in the first flare of May 1987 was determined.

A noticeable flare delay towards lower frequencies and step-by-step after-flare increase of the spectrum steepness was registered in a series of flares in May–June 1996. A rather different spectral and temporal character of successive flares also engages our attention.

Fig.10 shows the light curves of a very bright flare of SS433 in November 1999. At 2.25 and 2.3 GHz the data of GBI and RATAN-600 coincide, but at 8 GHz a noticeable difference is seen. In GBI data the fluxes at 8.3 GHz are underestimated by 10–15% resulting in a steeper average GBI spectrum of SS433 than it follows from our data. The duration of this flare indirectly indicates that the angular size of the source can be comparable to a synthesized beam pattern of the 2.4-km interferometer GBI, what results in a noticeable underestimation of the flux density at 8 GHz.

If we count off the start of the SS433 flare fading in November 1999 from the moment MJD5149.5, then we can try to determine the fading law. The analysis shows that it is preferable to choose a power law. The light curves at all frequencies show fading according to the law $\sim t^{-0.4}$ with a correlation factor exceeding 0.96 (Fig.11).

Fig.12 shows one of the obtained curves at a frequency of 3.9 GHz in long-term daily observations of SS433 in December 1999 – March 2000. Below in the diagram the alteration of spectral index is presented. An abrupt change of the index during two flares and a step-by-step after-flare increasing of the spectrum steepness due to more evident flux fall at high frequencies > 8 GHz is easily perceptible. It is in this after-flare part of the light curves where we detected a 6.05-day modulation with amplitude about 10% (Trushkin et al. 2001) possibly due to relativis-

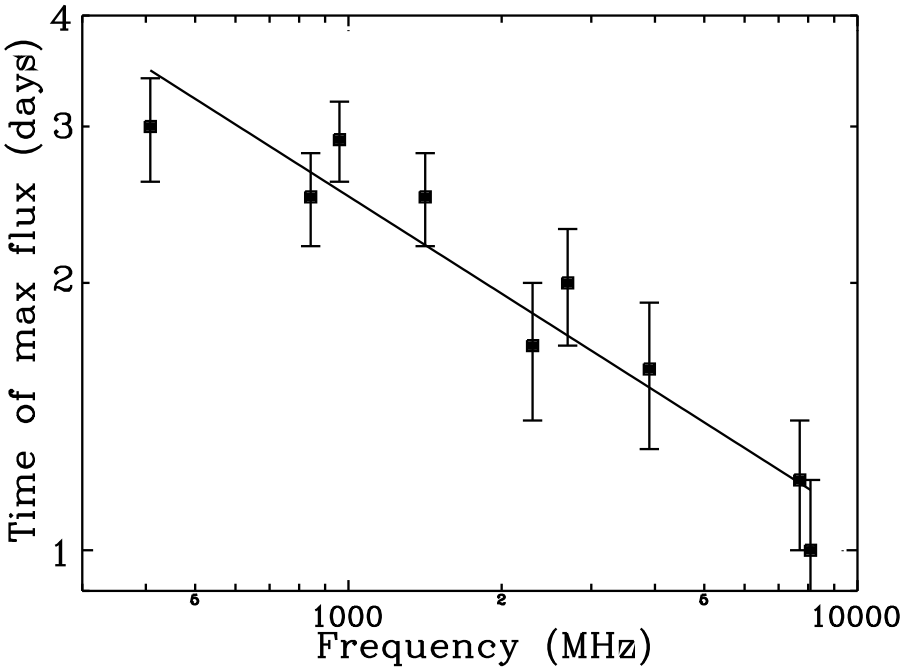

Figure 8: *The change of maximal flux times Δt_m with frequency of the SS433 flare in May 1987. Time is counted off an assumed flare onset on May 24 (JD 2446940.0). The line slope corresponds to a power law with an index of m = –0.36.*

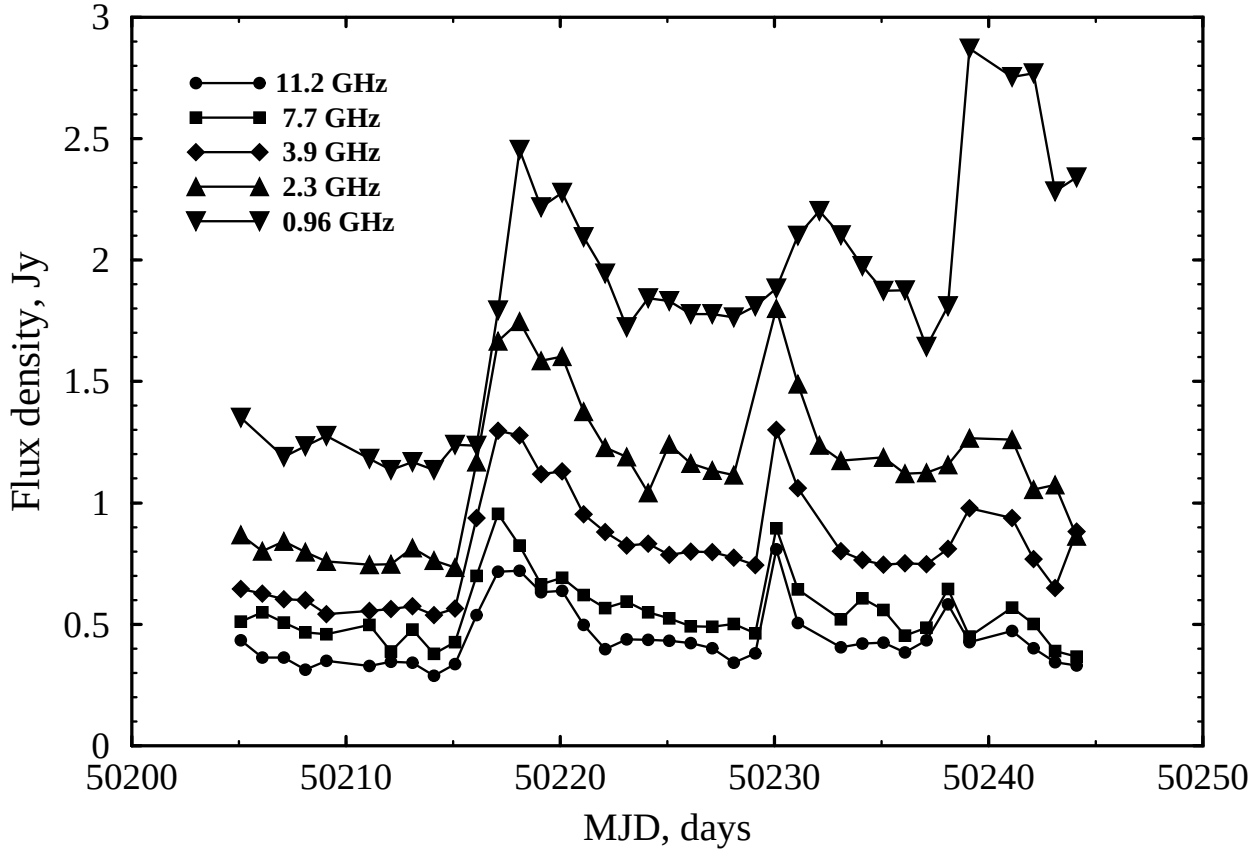

Figure 9: *The light curves during the flares of SS433 in May 1996.*

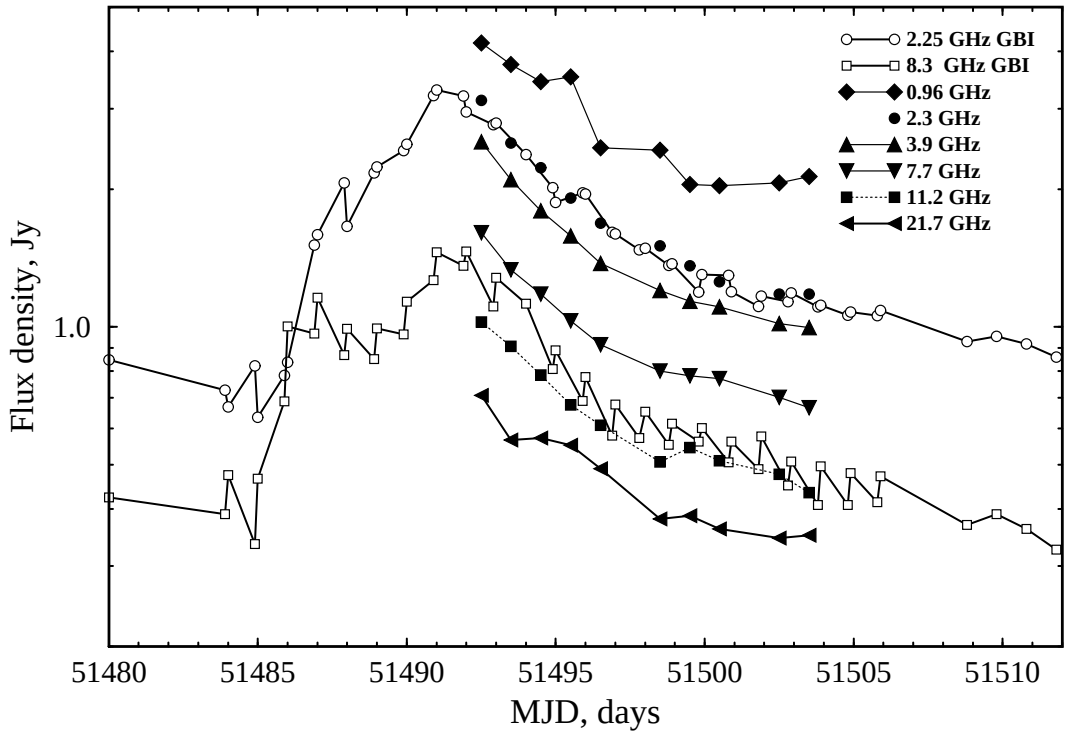

Figure 10: *The light curves of a very bright flare of SS433 in November 1999 by GBI data at 2.3 and 8.3 GHz and by RATAN-600 data at different frequencies.*

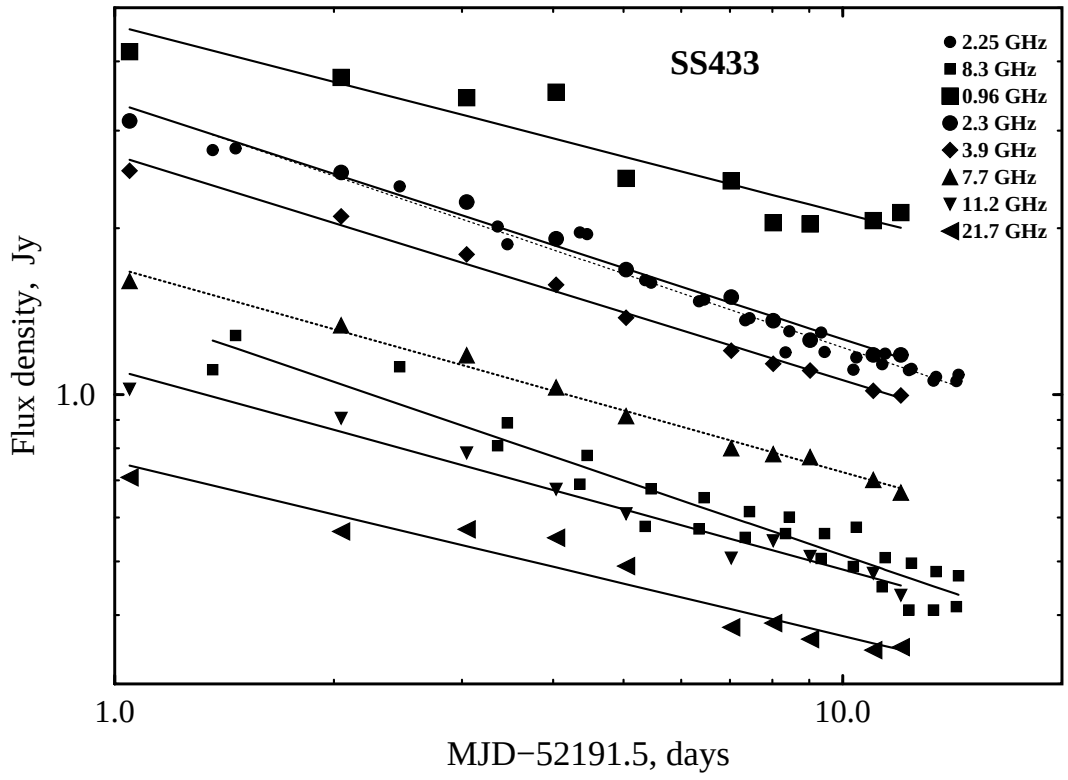

Figure 11: *The light curves of the SS433 flare in November 1999 after its maximum which are well approximated by power laws at different frequencies.*

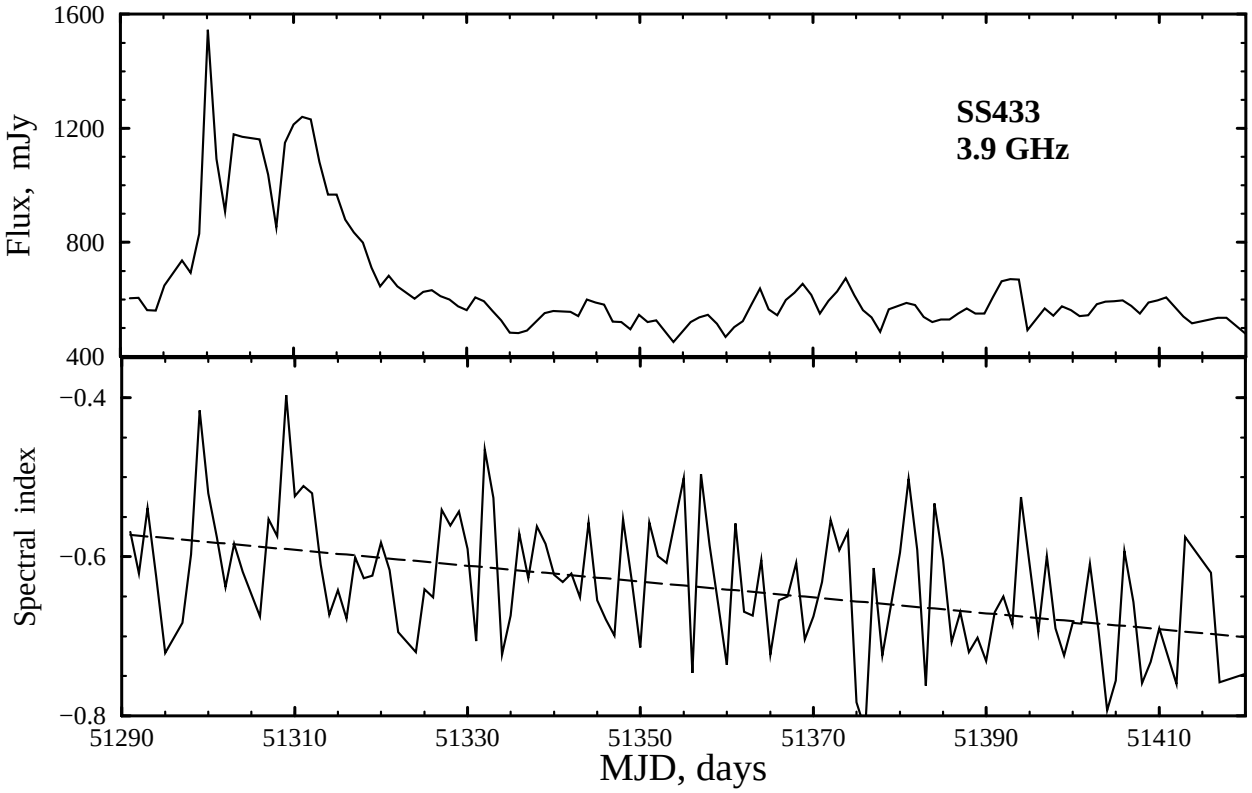

Figure 12: *The SS433 light curve at a frequency of 3.9 GHz (above) and variations of the spectral index (below) in December 1999 – March 2000.*

tic boosting of emission from jets in proportion to their "nodding" movements caused by the nutation of accreting disk and, correspondingly, the jets with a typical doubled frequency of orbital (13.08d) and precession motion. In order to illustrate such possibility we plotted in Fig.13 the predicted by kinematic model Doppler shifts around our set of 1999, allowed for the nodding motion (Vermeulen 1989). The flux variations more than five per cent are clearly seen in the sum of two fluxes from the receding and approaching jets, received for case of discrete blobs in jets. Additional effect could be obtained if the "lifetime" of these blobs is compatible with the 6-day period. The Fourier spectrum of this model curve show the presence of the 6.05-day harmonic.

3. Conclusion

This paper compile all observational data over many sets from December 1986 to January 2004 containing 940 observations of SS433 at two–six frequencies simultaneously. In all more than 4500 measurements of flux density at frequencies from 960 to 21700 MHz are presented. The average spectral index by all data is equal to –0.60 ± 0.14 with an average measurement error of 0.09 at an average flux density of 1.5 Jy at 960 MHz. In the indicated frequency range there were no cases of the spectrum inversion, when the spectral index would be positive. Thus, if there exists such a stage of the SS433 spectrum evolution, it is essentially shorter than one day not to get in such a moment during almost 1000 observations.

It was demonstrated that there are some earlier unknown regularities of the SS433 activity in the measured light curves. By the data on many flares the delay of flare maximum towards lower observational frequencies was detected. On the other side, the value of this maximum falls with frequency according to a power law. The flares fading with time also follows a power law. The indices of these relations change from flare to flare, but median values of indices coincide astonishingly well. They are equal to -0.4 ± 0.1. It is evidently an indication that the integral emission of the SS433 jets is due to similar properties of synchrotron radiation of the blobs–plasmons moving separately. In the end it is rigidly related with processes inside this XR and jets on the whole. From this point of view the models with inner shock waves propagating and increasing radio emission along the jet could be more preferable than the models in which the evolutions of separate radio components, blobs, are independent from each other.

The accumulated data of the flux density measurements are presented as publicly-accessible

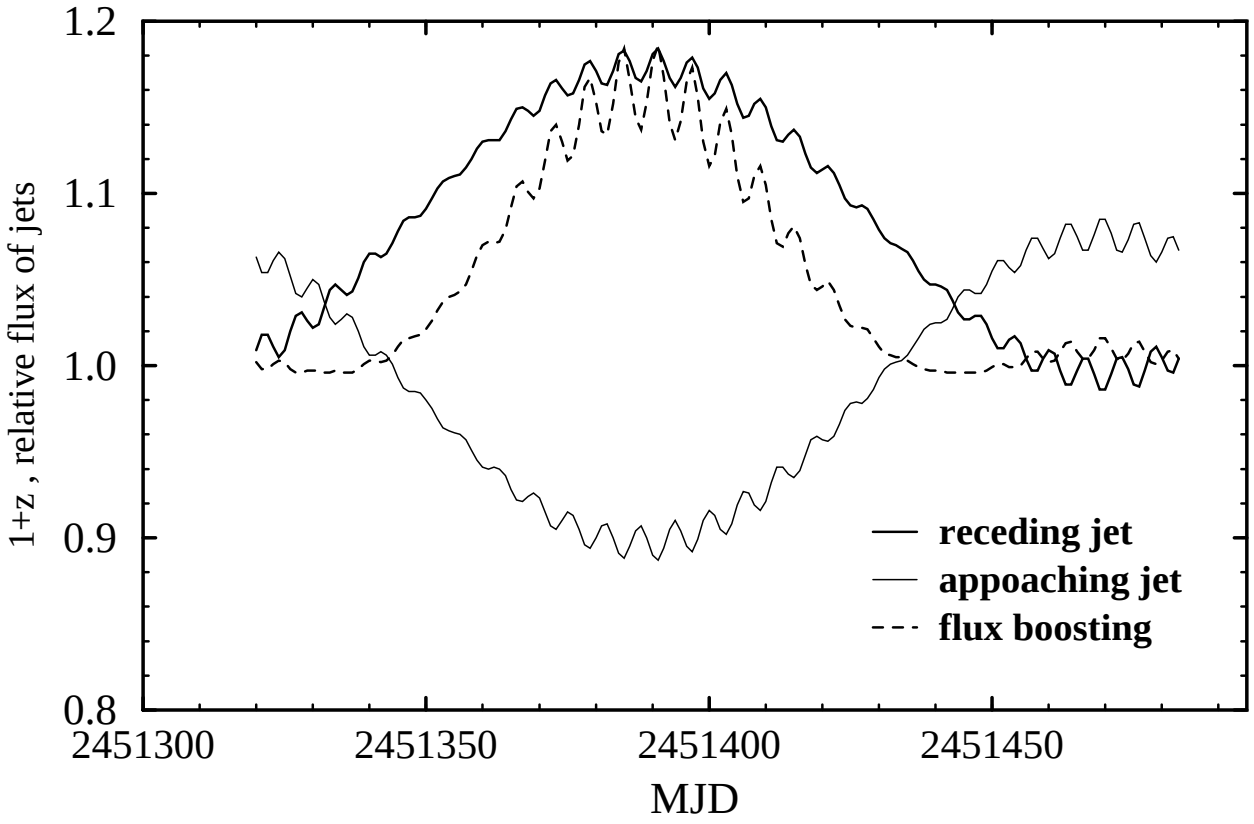

Figure 13: *Predicted by the kinematic model Doppler shifts during the May–July 1999 and relative flux variations of SS433, appeared due to the relativistic Doppler boosting.*

Web-programs for constructing the SS433 spectra in the Home Page of the data base CATS: http://cats.sao.ru/cgi-bin/ss433.cgi.

The complete data of all measurements carried out with RATAN-600 are presented in Table 3.

Acknowledgements. The work was carried out with the support of the RFBR grant 02-02-17439 in 2002-2004. The authors express their sincere gratitude to the RATAN-600 maintenance service for the good work of antenna and to our colleagues for the help in observations and processing of data. Also the authors are grateful to the GBI interferometer staff for a possibility of using their observational data of SS433.

References

Abell G.O., Margon B., 1979, Nature, **279**, 701

Aliakberov K.D., Mingaliev M.G., Naugolnaja M.N. et al., 1985, Astrofiz. Issled (Izv. SAO), **19**, 60

Baars J.W.M., Genzel R., Pauliny-Toth I.I.K., Witzel A., Astron. and Astrophys., 1977, **61** 99

Bursov N. N., Trushkin S.A., 1995, Astronomy Letters, **21**, 14

Cherepashchuk A. M., Sunyaev R. A., Seifina E. V., Panchenko I. E., Molkov S. V., Postnov K. A., 2003, Astron. and Astrophys., **411**, L441

Clark D. H., Murdin P., 1978, Nature, **276**, 44

Fender R., Rayner D., Norris R., Sault R.J., Pooley G., 2000, Astrophys. J., **530**, 29

Fender R.P., Rayner D., Trushkin S.A., O'Brein K., Sault R.J., Pooley G.G., Norris R.P., 2002, Mon. Not. R. Astron. Soc., **330**, 212

Fiedler R. L., Johnston K.J., Spencer J.H., Waltman E.B., Florkowski S. R., Matsakis D. N., Josties F. J., Angerhofer P. E., Klepczynski W. J., McCarthy, D. D., 1987, Astron. J., **94**, 1244

Garcia P.C., 1995. in: Proc. of YERAC-95, Cambridge U. Press.

Gladyshev S. A., 1981, Soviet Astron. Lett., **7**, 330

Gies D.R., Huang W., McSwain M.V., 2002a, Astrophys. J., **578**, L67

Gies D.R., McSwain M.V., Riddle R.L. et al., 2002b, Astrophys. J., **566**, 1069

Hjellming R.M., Brown R.L., Blankenship L.C., 1974, Astrophys. J., **194**, L13

Hjellming R.M., Johnston K.J., 1981, Nature, **290**, 100

Hjellming R.M., Johnston K.J., 1988, Astrophys. J., **328**, 600

Hjellming R.M., Rupen M.P., Hunstead R.W., Campbell-Wilson D. et al., 2000, Astrophys. J., bf 544, 977

Johnston K. J., Geldzahler B. J., Spencer J. H., Waltman E. B., Klepczynski W. J., Josties F. J., Angerhofer P. E., Florkowski D. R., McCarthy D.D., Matsakis D.N.,

1984, Astron. J., **89**, 509
Jowett F.H., Spencer R. E., 1995 in: The XXVIIth Young European Radio Astronomers Conference, ed.: D.A. Green and W. Steffen, in association with Cambridge University Press
Kotani T., Kawai N., Matsuoka M., Brinkmann W., 1996, Publ. of the Astron. Soc. of Japan, **48**, 619
Kotani T., Trushkin S., Denissyuk E. K., 2002, in: "New Views on MICROQUASARS", the Fourth Microquasars Workshop, Institut d'Etudes Scientifiques de Cargse, Corsica, France, May 27 – June 1, 2002. Ed.: Ph. Durouchoux, Y. Fuchs, and J. Rodriguez, Publ. by the Center for Space Physics: Kolkata (India), 257
Margon B., 1984, Ann. Rev. A&A, **22**, 507
Marti M., Paredes J.M., Estalella R., Astron. and Astrophys., 1992, **258**, 309
Margon B., Grandi S.A., Stone R.P.S., Ford H.C., Astrophys. J., 1979, **233**, L63
Marscher A.P., Brown R.L., Astrophys. J., 1975, **200**, 719
Marshall H.L., Canizares C.R., Schulz N.S., 2002, Astrophys. J., **564**, 941
McCormick D.G., Spencer R.E., Fender R.P., 2003 Astrophys. and Space Sci., **288**, 97
Mirabel F., Rodrigues I., 1999, Ann. Rev. A&A, **37**, 46
Mioduszewski A.J., Rupen M.P., Walker R.C., Taylor G.B., 2003, Astron. Astrophys. Suppl. Ser., **203**, 3105
Neizvestnyj S.I., Pustilnik S.A., Efremov V.G., 1980, Soviet Astron. Lett., **6**, 368
Ott M., Witzel A., Quirrenbach A. et al., 1994, Astron. Astrophys., **284**, 331
Paredes J.M., Marti M., Estalella R. et al., 1991, Astron. Astrophys., **248**, 124
Parijskii Yu.N., Korolkov D.V., 1986, Itogi Nauki i Tekhniki, Seria Astronomia (ISSN 0202-0742), **31**, 73
Shklovskij I.S., 1960, Astron. Zh., **37**, 945
Spencer R.E., 1079, Nature, **282**, 483
Spencer R.E., 1996, in: Radio emission from the stars and the sun. Proc. of a conf. Barcelona; Spain; 3-7 July 1995; ed: A.R. Taylor and J.M. Paredes, ASP Conf. Ser., **93**, 252
Stirling A.M., Jowett F.H., Spencer R.E., Paragi Z., Ogley R.N., Cawthorne T.V., 2002, Mon. Not. R. Astron. Soc., **337** 657
Trushkin S.A., 1989, Ph.D. Thesis
Trushkin S.A., 2000, Astron. and Astrophys. Trans., **19**, 524
Trushkin S.A., 1998, Astron. Letters, **24**, 16
Trushkin S.A., Bursov N.N., Smirnova Yu.V., 2001a, Astron. Reports, **45**, 804.
Trushkin S., Majorova E., Bursov N., 2001b, Astrophys. and Space Sci. Suppl., **276**, 135
Trushkin S.A., Bursov N.N., 2001, in: "Exploring the gamma-ray universe", Proc. of the Fourth INTEGRAL Workshop, 4-8 September 2000, Alicante, Spain. Ed.: B. Battrick, ESA SP-459, Noordwijk: ESA Publications Division, 2001, 445
van der Laan H., 1966, Nature, **211**, 1131
Verkhodanov O.V., Trushkin S.A., Andernach H., Chernenkov V.N., 1997, in: "Astronomical Data Analysis Software and Systems VI". Eds: G. Hunt and H. E. Payne, ASP Conf. Ser., **125**, 322
Vermeulen R.C. 1989, Ph.D Thesis, Un. Leiden. The Netherlands
Vermeulen R.C., McAdam W.B., Trushkin S.A. et al., 1993a, Astron. Astrophys., **270**, 189.
Vermeulen R.C., Schilizzi R.T., Spencer R.E. et al., 1993b, Astron. Astrophys., **270**, 177
Waltman E.B., Fiedler R.L., Johnston K.J. et al., 1994, Astron. J., **108**, 179
Waltman E.B., Fiedler R.L., Johnston K.J. et al., 1995, Astron. J., **110**, 290
Waltman E.B., Foster R.L., Pooley G.G. et al., 1996, Astron. J., **112**, 2690

Table 3: *Flux density measurements of SS 433*

MJD	Flux density in mJy at a frequency in GHz						Date	Sp.	Index
days	0.96	2.3	3.9	7.7	11.2	21.7	ddmmyy	Index	error
(1)	(2)	(3)	(4)	(5)	(6)	(7)	(8)	(9)	(10)
46767.48	2230	600	515	430			031286	−0.78	0.24
46768.48	1460	710	560	350			041286	−0.67	0.05
46769.48	1760	820	430	430			051286	−0.72	0.17
46770.47	1380	940	640	550			061286	−0.46	0.06
46771.47	1200	630	550	380			071286	−0.54	0.06
46773.46	1100		520	430			091286	−0.46	0.06
46774.46	1100		350	310			101286	−0.64	0.16
46775.46			518				111286		
46777.46		710	527				131286	−0.56	0.30
46778.45			482				141286		
46779.45	1200	470	500	370			151286	−0.54	0.17
46780.45	1080	670	550	490			161286	−0.38	0.07
46781.45	1620	810	675	510			171286	−0.55	0.08
46782.44	1560	770	530	360			181286	−0.71	0.04
46783.44	1070	420	470	370			191286	−0.48	0.19
46784.43	1280	610	770	460			201286	−0.44	0.16
46785.43	1660	1130	880	750			211286	−0.39	0.04
46787.43	2530	1890	1580	1230			231286	−0.34	0.01
46788.42	2530		1650	1320			241286	−0.31	0.01
46789.42	2850	2200	1450	1150			251286	−0.46	0.06
46790.42	3090	1800	1330	1000			261286	−0.55	0.04
46791.42	3050	1680	1260	900			271286	−0.59	0.04
46792.41	2900	1420	1115	840			281286	−0.59	0.08
46793.41	2410	1320	1070	760			291286	−0.55	0.04
46794.41	2080	1000	825	750			301286	−0.49	0.13
46795.40	2150	930	775	590			311286	−0.61	0.11
46796.40	2260	1000	720	550			010187	−0.68	0.10
46797.40	2260	950	670	550			020187	−0.69	0.12
46798.40	1950		650	520			030187	−0.66	0.11
46799.39	1690	750	645	510			040187	−0.57	0.12
46800.39	1200		608	500			050187	−0.43	0.05
46801.39	2000	860	700	900			060187	−0.41	0.24
46802.38	1350	1130	1300	1100			070187	−0.08	0.06
46803.38	2170	1690	1190	1000			080187	−0.39	0.05
46804.38	2600	1850	1180	950			090187	−0.51	0.06
46805.37	2400	1420	1070	890			100187	−0.49	0.06
46806.37	2590	1330	930	790			110187	−0.58	0.09
46807.37	2570	1820	1140	820			120187	−0.57	0.06
46808.37	2650	1690	1190	720			130187	−0.62	0.04
46809.37	2930	1480	1165	660			140187	−0.70	0.04
46810.36	3530	1350	1065	610			150187	−0.82	0.09
46812.36	3100	1230	1000	700			170187	−0.70	0.11
46814.36	2620	1210	875	370			190187	−0.92	0.08
46817.36	1700	1080	1060	680			220187	−0.41	0.07
46820.35	2600	1800	1630				250187	−0.34	0.06
46822.34	2830	1320	1005	680			270187	−0.68	0.06
46824.34	2050	950	515	530			290187	−0.69	0.18

Table 3: *Flux density measurements of SS 433 (continued)*

(1)	(2)	(3)	(4)	(5)	(6)	(7)	(8)	(9)	(10)
46827.33	1550	750	435	500			010287	−0.59	0.19
46829.33	1600	600	615	510			030287	−0.53	0.19
46831.33	1340	780	650	500			050287	−0.47	0.05
46832.32	1130	910	560	520			060287	−0.41	0.09
46834.31	1240	780	615	580			080287	−0.38	0.08
46836.30	1550	860	595				100287	−0.68	0.01
46837.30	1300	800	650	370			110287	−0.59	0.06
46838.30	1200	850	630	540			120287	−0.40	0.04
46839.30	1500	1010	655	500			130287	−0.55	0.05
46840.29	1390	950	685	330			140287	−0.68	0.11
46843.29	1600	1270	1020	840			170287	−0.31	0.02
46844.28	2000	1220	1070	910			180287	−0.38	0.06
46845.28	1840	1100	920	710			190287	−0.45	0.04
46846.28	1850	1160	860	440			200287	−0.68	0.08
46847.28	1760	1070	895	440			210287	−0.64	0.10
46849.27	2530	1500	1230	800			230287	−0.54	0.03
46850.27	2400	1800	1440	800			240287	−0.51	0.09
46851.27	2400	1720	1385	770			250287	−0.53	0.09
46852.27	2450	1440	1160	585			260287	−0.67	0.08
46853.27	1980	1400	900	400			270287	−0.76	0.14
46854.27	2130	1240	815	350			280287	−0.85	0.11
46856.27	1430	750	585	260			020387	−0.79	0.09
46857.26	1460	960	535	340			030387	−0.72	0.08
46858.26	1800	680	540	320			040387	−0.81	0.09
46859.26	1350	1020	655	370			050387	−0.63	0.10
46860.26	1150	1020	780	470			060387	−0.43	0.11
46935.29	1300	810	620	370			200587	−0.59	0.04
46936.29	1300	660	640	420			210587	−0.52	0.09
46937.29	1120	760	600	530			220587	−0.37	0.05
46938.28		630	480	420			230587	−0.33	0.09
46939.28	1080	610	480	440			240587	−0.44	0.09
46940.28	1150	630	490	540			250587	−0.38	0.15
46941.27	1350	1030	1120	650			260587	−0.31	0.12
46942.27	1720	1010	0930	470			270587	−0.59	0.10
46943.27	1760	1150	1070	700			280587	−0.42	0.05
46944.27	1800	1460	1260	770			290587	−0.39	0.09
46945.26	1850	1460	1020	680			300587	−0.49	0.07
46946.26	1730	1200	960	600			310587	−0.50	0.05
46947.26	1650	1060	870	560			010687	−0.51	0.03
49445.153	1550	630	415	339	326		030494	−0.63	0.12
49446.150	1060	730	445	385	255		040494	−0.56	0.06
49447.147	1120	590	455	316	245		050494	−0.60	0.03
49449.142	1170	650	540	299	278		070494	−0.60	0.04
49450.139	1280	780	520	328	332		080494	−0.59	0.05
49451.136	1100	610	558	328	302		090494	−0.53	0.05
49452.133	870	590	590	397	279		100494	−0.43	0.07
49453.130	1340	640	527	374	293		110494	−0.59	0.05
49454.128	1010	670	536	425	251		120494	−0.52	0.07

Table 3: *Flux density measurements of SS 433 (continued)*

(1)	(2)	(3)	(4)	(5)	(6)	(7)	(8)	(9)	(10)
49455.125	1090	670	487	293	251		130494	−0.62	0.02
49456.123	1220	730	509	391	217		140494	−0.65	0.07
49457.120	1100	720	545	362	316		150494	−0.52	0.01
49458.117	1430	980	647	460	316		160494	−0.61	0.05
49459.114	1510	950	799	684	335		170494	−0.53	0.11
49460.112	1540	1030	839	690	335		180494	−0.54	0.11
49461.109	1750	1150	866	690	476		190494	−0.50	0.04
49462.106	2380	1450	999	858	790		200494	−0.45	0.06
49463.104	2150	1330	926	673	575		210494	−0.55	0.02
49464.101	2580	1550	1286	1072	820		220494	−0.44	0.04
49465.098	2900	1910	1451	966	804		230494	−0.53	0.01
49466.096	2950	1910	1438	1029	762		240494	−0.54	0.02
49467.093	2870	1500	1268	960	808		250494	−0.50	0.05
49468.090	2640	1230	973	638	488		260494	−0.67	0.04
49469.087	2200	1114	830	477	475		270494	−0.65	0.05
49470.084	2020	960	741	449	282		280494	−0.76	0.05
49471.081	2190	1570	1455	1196	978		290494	−0.31	0.03
49472.079	2360	1730	1188	914	631		300494	−0.52	0.05
49473.076	2510	1450	1125	802	609		010594	−0.56	0.02
49474.073	2440	1340	1045	732	577		020594	−0.57	0.02
49475.070	2210	1070	848	604	336		030594	−0.70	0.08
49476.068	1850	910	741	540	368		040594	−0.61	0.05
49477.066	1720	1010	714	405	337		050594	−0.68	0.03
49478.063	1660	890	643	322	228		060594	−0.81	0.05
49479.061	1560	850	634	431	334		070594	−0.62	0.02
49480.059	1450	840	647	443	292		080594	−0.62	0.04
49481.056	1400	810	621	420	315		090594	−0.59	0.02
49482.054	1550	760	567	454	274		100594	−0.65	0.07
49483.052	1600	910	563	399	258		110594	−0.72	0.04
49484.049	1240	710	710	335	326		120594	−0.56	0.08
49485.045	1240	1015	550				130594	−0.55	0.25
49486.043	1290	850	600				140594	−0.54	0.05
49487.041	1540	680	530				150594	−0.78	0.12
49488.038	1395	700	540				160594	−0.69	0.08
49489.036	1410	750	560				170594	−0.67	0.05
49490.033	1400	670	500				180594	−0.75	0.08
49491.031	1360	820	550				190594	−0.64	0.05
49492.028	1460	880	600				200594	−0.63	0.04
49493.026	1400	760	620				210594	−0.59	0.08
49494.023	1490	730	550				220594	−0.72	0.08
49495.020	1350	700	560				230594	−0.64	0.09
49496.018	1340	630	600				240594	−0.60	0.20
49497.016	1520	700	550				250594	−0.74	0.11
50205.08	1350	868	646	511	434		020596	−0.46	0.02
50206.08		802	627	549	363		030596	−0.45	0.10
50207.08	1190	842	604	507	363		040596	−0.46	0.04
50208.08	1234	798	599	467	313		050596	−0.53	0.04
50209.08	1276	758	542	459	350		060596	−0.51	0.04

Table 3: *Flux density measurements of SS 433 (continued)*

(1)	(2)	(3)	(4)	(5)	(6)	(7)	(8)	(9)	(10)
50211.08	1181	746	555	497	328		070596	−0.48	0.05
50212.05	1136	748	563	387	345		080596	−0.50	0.02
50213.05	1168	815	574	479	341		090596	−0.48	0.04
50214.05	1136	763	538	379	287		100596	−0.56	0.02
50215.05	1239	733	564	426	335		110596	−0.52	0.02
50216.05	1236	1168	937	700	537		120596	−0.34	0.07
50217.05	1793	1666	1297	954	716		130596	−0.38	0.07
50218.05	2454	1747	1277	824	720		140596	−0.52	0.03
50219.05	2217	1586	1118	664	631		150596	−0.55	0.05
50220.05	2277	1602	1129	692	638		160596	−0.55	0.04
50221.05	2094	1375	952	621	498		170596	−0.60	0.02
50222.05	1944	1228	879	567	397		180596	−0.64	0.04
50223.05	1724	1189	825	593	437		190596	−0.56	0.03
50224.05	1843	1042	831	549	435		200596	−0.58	0.02
50225.05	1832	1241	785	525	432		210596	−0.61	0.04
50226.05	1777	1163	800	492	422		220596	−0.61	0.03
50227.05	1777	1133	798	490	401		230596	−0.62	0.02
50228.05	1765	1115	775	502	341		240596	−0.66	0.04
50229.05	1811		744	463	381		250596	−0.64	0.01
50230.05	1883	1800	1301	896	808		260596	−0.38	0.07
50231.05	2101	1489	1061	643	506		270596	−0.60	0.05
50232.05	2203	1238					280596	−0.66	0.20
50233.05	2103	1174	801	520	406		290596	−0.67	0.01
50234.05	1975		764	607	420		300596	−0.61	0.05
50235.05	1873	1187	745	559	425		310596	−0.61	0.03
50236.05	1876	1120	751	454	384		010696	−0.67	0.02
50237.05	1643	1124	748	485	434		020696	−0.57	0.04
50238.05	1810	1156	810	646	582		030696	−0.47	0.04
50239.05	2872	1267	977	449	427		040696	−0.80	0.06
50241.05	2754	1260	938	569	473		060696	−0.71	0.04
50242.05	2769	1054	768	502	402		070696	−0.76	0.07
50243.05	2283	1074	650	390	343		080696	−0.79	0.05
50244.05	2341	862	881	366	330		090696	−0.79	0.10
50565.128	1510	567	508	264	252		270497	−0.73	0.09
50568.120	600	568	480	255	280		300497	−0.38	0.10
50569.117	1132	565	426	380	250		010597	−0.56	0.07
50570.115			319	270	125		020597	−0.81	0.30
50571.112	1036	397	281	250	142		030597	−0.73	0.11
50573.107	952	411	268	320	125		050597	−0.69	0.17
50574.104	600	406	331	320	200		060597	−0.39	0.07
50575.101	1079	478	336	470	233		070597	−0.50	0.17
50576.098	716		347	590			080597	−0.16	0.32
50577.096	987	488	322	490	175		090597	−0.55	0.20
50578.093	1072	479	339	290	250		100597	−0.57	0.09
50579.090	899	489	410	280	242		110597	−0.53	0.03
50580.087	767	593	445	320	250		120597	−0.46	0.04
50581.085	653	557	395	430	208		130597	−0.39	0.13
50582.082	780	599	389	460	275		140597	−0.37	0.10

Table 3: *Flux density measurements of SS 433 (continued)*

(1)	(2)	(3)	(4)	(5)	(6)	(7)	(8)	(9)	(10)
50583.079	980	674	422	470	267		150597	−0.47	0.10
50584.077	749	591	408	530	275		160597	−0.33	0.12
50585.074			432				170597		
50589.063	722	611	476	290	233		210597	−0.48	0.07
50591.057	1599	553	389	270	267		230597	−0.73	0.12
50593.052	723	565	425	370	233		250597	−0.43	0.07
50597.041	375	546	431	300	225		290597	−0.23	0.15
50599.036	602	535	391	270	192		310597	−0.47	0.08
50601.030	1125	667	502	310	233		020697	−0.64	0.02
50603.025	957	654	412	380	225		040697	−0.55	0.08
50604.022	1153	585	446	320	208		050697	−0.66	0.05
50605.019	699	625		270	200		060697	−0.53	0.10
50607.014	999	649	440		242		080697	−0.58	0.03
50609.008	863	638	441	240	192		100697	−0.64	0.07
50611.003	1118	605	405		225		120697	−0.65	0.03
50612.997	922	558	425	270	225		140697	−0.58	0.01
50614.992	1124	488	377	220	167		160697	−0.76	0.04
50616.986	879	571	453	140	200		180697	−0.72	0.16
50618.981	1072	613	355	170	183		200697	−0.79	0.09
50620.976	1077	528	345	110	192		220697	−0.85	0.19
50622.970	891	524	312	210	192		240697	−0.66	0.05
50624.968	1765	627	441	250	233		260697	−0.83	0.09
50626.963	1716	625	475	250	233		280697	−0.82	0.08
50627.960	1451	562	381	190	233		290697	−0.80	0.12
50629.954	790	481	429	170	200		300697	−0.63	0.11
50630.948	1641	536	395	250	233		020797	−0.79	0.11
50634.937	1554	524	364	180	225		060797	−0.84	0.14
50636.932	639	671	420		200		080797	−0.50	0.15
50639.924	699		229	120			100797	−0.84	0.04
50640.921	1159	454	371	170	150		120797	−0.84	0.07
50642.915	1257	488	367	220	217		140797	−0.72	0.09
50644.910	956	473	361	260	192		160797	−0.63	0.04
50646.905	975	490	343	180	150		180797	−0.78	0.03
50648.899	976	528	385	270	225		200797	−0.59	0.03
50650.894	1116	505	379	290	175		220797	−0.69	0.07
50654.883	841	475	343	200	150		260797	−0.70	0.02
50656.877	593	449	414	210	175		280797	−0.51	0.09
50659.869	858	598	400	290	208		300797	−0.57	0.04
50661.864	928	575	403	360	217		010897	−0.54	0.07
50663.858	764	391	296	190	175		030897	−0.61	0.04
50665.853	841	447	382	250	192		050897	−0.58	0.04
50667.847	829	453	361	290	192		070897	−0.55	0.05
50669.842	960	420	329	230	158		090897	−0.69	0.06
50671.836	908	455	424	330	233		110897	−0.50	0.07
50672.833	945	571	450	390	258		120897	−0.48	0.05
50673.830	1090	632	484	350	267		130897	−0.56	0.02
50674.827	959	585	381	370	208		140897	−0.56	0.09
50675.823	982	638	341	290	183		150897	−0.67	0.07

Table 3: *Flux density measurements of SS 433 (continued)*

(1)	(2)	(3)	(4)	(5)	(6)	(7)	(8)	(9)	(10)
50676.820		423	377	310			160897	−0.26	0.02
50677.817		423	411	280			170897	−0.35	0.14
50679.814		425	425	330			180897	−0.22	0.10
50680.811		531	400	340			190897	−0.36	0.08
50681.808		414	345	220			200897	−0.53	0.09
50682.805		394	373	260			210897	−0.35	0.12
50683.802		444	387	320			220897	−0.27	0.00
50685.800		564	434	370			230897	−0.34	0.07
50686.797		625	468	400			240897	−0.36	0.09
51291.10	1230	825	604	377	300	225	230499	−0.57	0.02
51292.10	1395	840	605	366	315	205	240499	−0.62	0.01
51293.09	1330	725	563	384	300	256	250499	−0.54	0.04
51294.09	1345	820	561	378	270	203	260499	−0.62	0.02
51295.09	1370	760	649		310	129	270499	−0.72	0.08
51297.08	1250	906	737		420	126	290499	−0.68	0.14
51298.08	1535	970	694	400	370	250	300499	−0.60	0.03
51299.08	1462	925	830				010599	−0.42	0.09
51300.08	2050	1615	1545		570	470	020599	−0.52	0.09
51301.07	2230	1644	1092		551	405	030599	−0.58	0.04
51302.07	2372	1420	908	642	498		040599	−0.64	0.02
51303.06	2565	1771	1179	873	691	405	050599	−0.58	0.03
51304.06	1977	1846	1170	823	611	288	060599	−0.62	0.09
51306.05	2466	1534	1161	677	564	289	080599	−0.68	0.04
51307.05	2332	1477	1038	717	623	413	090599	−0.55	0.01
51308.04	2210	1293	853	530	668	336	100599	−0.57	0.07
51309.04	2078	1430	1149	1005	997	503	110599	−0.40	0.06
51310.03	2038	1635	1214	933	686	385	120599	−0.52	0.06
51311.03	2253	1915	1240	870	755	481	130599	−0.51	0.04
51312.02	2195	1881	1231	843	743	453	140599	−0.52	0.05
51313.02	3143	1753	1082	718	625	498	150599	−0.61	0.05
51314.02	3042	1499	967	675	541	363	160599	−0.67	0.03
51315.02	2175	1383	967	610	461	306	170599	−0.64	0.02
51316.02	2526	1221	879	554	451	297	180599	−0.68	0.02
51317.02	2318	1175	835	520	483	358	190599	−0.60	0.04
51318.01	2106	1091	799	573	519	256	200599	−0.63	0.05
51319.01	1987	1127	711	509	423	281	210599	−0.62	0.03
51320.01	1860	980	646	474	359	319	220599	−0.58	0.05
51321.02	2038	950	683	454	380	296	230599	−0.62	0.05
51322.01	1652	949	646	418	316	186	240599	−0.69	0.01
51324.01	1526	906	602	405	335	144	250599	−0.72	0.06
51325.01	1659	896	626	459	376	202	270599	−0.64	0.03
51326.01	1835	874	633	417	371	222	280599	−0.65	0.03
51327.01	1318	849	611	423	355	246	290599	−0.54	0.01
51328.01	1461	894	600	427	359	258	300599	−0.56	0.02
51329.01	1431	871	576	416	359	268	310599	−0.54	0.03
51330.00	1580	874	563	435	339	249	010699	−0.59	0.03
51331.00	1386		607	424	364	125	020699	−0.71	0.12
51331.99	1212	822	593	389	369	136	030699	−0.71	0.12

Table 3: *Flux density measurements of SS 433 (continued)*

(1)	(2)	(3)	(4)	(5)	(6)	(7)	(8)	(9)	(10)
51332.99	1372	810	559	437	355	341	040699	−0.47	0.05
51333.99	1090	788	527	376	345	209	050699	−0.53	0.03
51334.99	1452	699	483	347	367	112	060699	−0.72	0.10
51335.98	1380	722	482	305	241	174	070699	−0.67	0.03
51336.98	1173	722	491	340	291	199	080699	−0.57	0.02
51337.97		716	521	331	287	171	090699	−0.63	0.03
51338.97	1412	748	552	398	339	233	100699	−0.56	0.03
51339.97	1419	726	559	412	367	199	110699	−0.58	0.04
51340.96	1357	748	558	373	291	189	120699	−0.62	0.01
51341.96	1370	807	556	328	263	210	130699	−0.63	0.03
51342.95	1344	804	542	378	280	199	140699	−0.62	0.01
51343.95	1280	817	600	371	334	155	150699	−0.65	0.05
51344.93	1377	758	589	428	321	238	160699	−0.56	0.02
51345.93	1723	789	582	356	349	205	170699	−0.65	0.05
51346.92	1699	809	522	361	335	184	180699	−0.68	0.05
51347.92	1513	674	520	367	353	130	190699	−0.70	0.08
51348.92	1122	673	495	361	277	199	200699	−0.55	0.01
51349.91	1209	750	546	383	314	154	210699	−0.63	0.05
51350.91	1372	732	520	389	305	121	220699	−0.71	0.07
51351.91	1199	703	527	397	292	206	230699	−0.56	0.02
51352.90		595				155	240699	−0.60	1.45
51353.90	1097	661	450	330	248	162	250699	−0.61	0.02
51355.89	1138	702	520	361	281	260	270699	−0.50	0.04
51356.89		768	537	366	362	121	280699	−0.75	0.15
51357.89	1208	723	546	359	305	278	290699	−0.50	0.04
51358.89	1212	746	515	381	304	187	300699	−0.59	0.02
51359.88	1232	677	469	346	255	146	010799	−0.66	0.03
51360.88	1229	639	503	344	264	101	020799	−0.74	0.08
51361.88	1102	754	524	358	260	212	030799	−0.56	0.03
51362.87	1491	731	582	380	346	155	040799	−0.67	0.06
51363.87	1109	775	639	426	259	129	050799	−0.67	0.09
51364.87	1180	767	566	406	280	178	060799	−0.60	0.03
51365.86	1339	741	544	389	255	127	070799	−0.72	0.06
51366.86	1336	844	598	358	281	180	080799	−0.65	0.02
51367.86	1290	803	623	424	315	155	090799	−0.65	0.06
51368.85	1358	908	654	427	346	202	100799	−0.61	0.03
51369.85	1093	864	616	412	323	105	110799	−0.70	0.12
51370.85	1342	772	550	393	343	136	120799	−0.68	0.07
51371.85	1436	751	595	407	326	180	130799	−0.63	0.03
51372.84	1467	861	628	446	362	259	140799	−0.55	0.01
51373.84	1333	874	674	436	380	197	150799	−0.59	0.04
51374.84	1154	821	614	449	336	187	160799	−0.57	0.05
51375.83	1291	730	563	373	285	89	170799	−0.78	0.11
51376.83	1201	678	537	339	251	74	180799	−0.82	0.12
51377.83	1030	659	487	376	196	163	190799	−0.61	0.06
51378.83	1384	679	566	400	334	108	200799	−0.72	0.10
51380.83	1302	776	588	393	356	185	220799	−0.60	0.04
51381.83	1273	712	580	381	287	293	230799	−0.50	0.05

Table 3: *Flux density measurements of SS 433 (continued)*

(1)	(2)	(3)	(4)	(5)	(6)	(7)	(8)	(9)	(10)
51382.83	1267	764	539	399	337	183	240799	−0.59	0.03
51383.83	1194	742	521	372	269	92	250799	−0.76	0.10
51384.83	1054	702	529	308	290	214	260799	−0.53	0.03
51385.83	1135	714	529	323	285	171	270799	−0.60	0.02
51386.83	1338	731	551	348	238	145	280799	−0.71	0.03
51387.83	1273	804	568	352	305	148	290799	−0.67	0.05
51388.83	1413	738	550	345	263	139	300799	−0.72	0.03
51389.82	1171	768	550	346	264	124	310799	−0.70	0.06
51390.82		896	609	391	316	165	010899	−0.73	0.04
51391.82	1681	885	664	469	313	199	020899	−0.67	0.03
51392.82	1325	878	671	437	400	148	030899	−0.65	0.09
51393.81	1789	887	670	463	356	188	040899	−0.69	0.04
51394.80	1058	738	493	337	287	221	050899	−0.52	0.03
51396.80	1281	771	568	373	283	134	070899	−0.69	0.05
51397.80	1161	749	543	391	303	169	080899	−0.60	0.04
51398.79	1060		576	406	353	93	090899	−0.69	0.18
51399.79	1379	794	563	387	286	128	100899	−0.72	0.06
51400.79	1247	789	541	395	358	119	110899	−0.68	0.10
51401.79	1166	763	544	347	326	118	120899	−0.68	0.09
51402.79	1317	771	583	371	316	191	130899	−0.61	0.02
51403.78	1484	818	592	405	339	147	140899	−0.69	0.06
51404.78	1546	841	593	435	352	97	150899	−0.79	0.12
51405.78	1317	834	597	380	287	110	160899	−0.76	0.08
51406.77	1152	781	577	399	276	186	170899	−0.59	0.03
51407.77	1171	729	550	359	305	134	180899	−0.66	0.06
51408.77	1251	801	589	334	228	118	190899	−0.76	0.06
51409.77	1195	801	596	386	262	112	200899	−0.73	0.09
51410.76	1340	944	607	447	291	152	210899	−0.69	0.06
51412.76	1424	766	540	334	319	109	230899	−0.76	0.08
51413.76	1312	842	516	362	293	237	240899	−0.57	0.04
51416.75	1358	753	536	366	253	208	270899	−0.62	0.03
51417.75	1169	765	535	352	279	93	280899	−0.76	0.10
51420.75	1298	589	458	272	180	127	310899	−0.75	0.03
51421.75	1116	715	435	253	281	49	010999	−0.90	0.17
51492.548	4170	3124	2538	1606	1024	709	101199	−0.59	0.06
51493.545	3744	2523	2099	1334	906	566	111199	−0.61	0.05
51494.542	3438	2229	1792	1179	785	572	121199	−0.59	0.04
51495.539	3522	1913	1581	1031	675	555	131199	−0.61	0.04
51496.537	2461	1684	1377	914	610	379	141199	−0.60	0.05
51498.531	2432	1502	1200	801	507	268	161199	−0.69	0.06
51499.528	2047	1361	1138	781	545	387	171199	−0.54	0.03
51500.526	2036	1256	1106	771	510	362	181199	−0.55	0.04
51502.520	2062	1180	1017	702	476	345	201199	−0.57	0.03
51503.517	2132	1180	997	666	434	436	211199	−0.54	0.05
51657.097	686	858	472	350	293	272	230400	−0.38	0.09
51659.092	1228	706	545	431	374	143	250400	−0.61	0.09
51661.086	1625	952	644	480	378	348	270400	−0.52	0.05
51663.081		869	578	495	406	309	290400	−0.44	0.04

Table 3: *Flux density measurements of SS 433 (continued)*

(1)	(2)	(3)	(4)	(5)	(6)	(7)	(8)	(9)	(10)
51664.078	967	831	679	463	358	267	300400	−0.44	0.05
51665.075	1305	887	749	567	480	661	010500	−0.27	0.08
51666.072	1689	829	694	541	430	240	020500	−0.57	0.05
51667.070	1191	814	609	522	456	261	030500	−0.45	0.04
51668.067	1247	791	659	417	399	477	040500	−0.36	0.08
51669.064	2002	634	587	422	317	170	050500	−0.71	0.08
51670.062	1021	520	534	412	350	252	060500	−0.41	0.05
51671.059	1316	955	527	385	350	166	070500	−0.65	0.06
51673.053	1954	774	564	413	354	150	090500	−0.74	0.07
51674.051	1945	532	539	381	302	173	100500	−0.69	0.10
51675.048	2400	786	528	376	323		110500	−0.80	0.11
51676.045	1295	597	578	460	400	235	120500	−0.48	0.06
51677.042	2524	812	623	462	410	341	130500	−0.61	0.11
51678.040	1768	838	638	520	451	144	140500	−0.70	0.11
51679.037	1618	825	649	485	372	269	150500	−0.56	0.03
51680.034	2205	872	624	426	328	196	160500	−0.74	0.05
51681.032	1227	1090	513	366	296	126	170500	−0.73	0.09
51682.029	1815	834	507	395	334	156	180500	−0.73	0.06
51683.026	1185	1283	573	414	364	212	190500	−0.59	0.09
51684.023	3305	1529	597	480	360	262	200500	−0.83	0.10
51685.021	831	824	581	448	362	183	210500	−0.48	0.09
51740.909	914		502	350	240		160700	−0.52	0.06
51742.904	995		548	380	250		180700	−0.53	0.07
51744.898	762	1002	565	360	305		200700	−0.44	0.15
51746.893	780	926	490	258	250		220700	−0.56	0.15
51748.888	1200	519	435				240700	−0.75	0.17
51883.477			492	362	519		051200	−0.01	0.36
51885.472			603	363	344		071200	−0.56	0.16
51886.469			585	339	247		081200	−0.81	0.01
51887.466			461	343	327		091200	−0.34	0.08
51888.464	2000		662	381	429		101200	−0.68	0.11
51889.461			529	324	267		111200	−0.66	0.05
51890.458	1299		597	336	264		121200	−0.65	0.04
51892.453	1795		529	367	299		141200	−0.74	0.06
51894.447	1183		499	417	269		161200	−0.57	0.07
51895.444	828		487	560	265		171200	−0.37	0.17
51897.439	930		574	486	239		191200	−0.47	0.15
51898.436			580	427	237		201200	−0.80	0.29
51899.434	1443			578	186		211200	−0.70	0.33
51900.431	1487		521	570	356		221200	−0.53	0.12
51901.428	1510		562	583	285		231200	−0.60	0.14
51902.425	1305		560	702	333		241200	−0.46	0.17
51904.420			515	405	251		261200	−0.64	0.24
51905.417	751		565	420	203		271200	−0.45	0.18
51906.414			565	507	328		281200	−0.47	0.26
51907.412			607	514	350		291200	−0.49	0.20
51909.406			492				311200		
51913.395	1852		1682	1450	1342	906	040101	−0.21	0.06

Table 3: *Flux density measurements of SS 433 (continued)*

(1)	(2)	(3)	(4)	(5)	(6)	(7)	(8)	(9)	(10)
51914.393	2238		1560	1024	805	493	050101	−0.48	0.07
51915.390	2317	1597	1081	674	568	443	060101	−0.56	0.03
51916.387	2457	1606	978	575	485	294	070101	−0.70	0.03
51918.382	2467	1361	782		402	226	090101	−0.76	0.03
51919.379	2092	1117	722	411	341		100101	−0.76	0.02
51920.376	1723	1200	705	375	375	239	110101	−0.67	0.05
51921.373	2099	1132	666	459	359	330	120101	−0.63	0.07
51922.371	1490	982	769		306	275	130101	−0.59	0.06
51923.368	1905	1270	712	343	271	255	140101	−0.73	0.09
51925.363	1617	998	574	304	336	143	160101	−0.76	0.07
51926.360	1532	919	552	329	261		170101	−0.74	0.03
51928.354	1344	805	526	370	321		190101	−0.60	0.03
51930.349	1713	933	598	407	368	227	210101	−0.64	0.03
51932.343	1357	1072	632	416	371	155	230101	−0.68	0.08
51934.338	1638	1011	600	348	370	145	250101	−0.75	0.07
51936.333	1323	762	626	416	393	269	270101	−0.50	0.03
51940.322	1528	782	577	372	313	242	310101	−0.60	0.04
51942.316	1234	871	577	437	396		020201	−0.49	0.04
51944.311	1180	817	631		294		040201	−0.57	0.06
51946.305	2160	773	623	395	351		060201	−0.72	0.09
51948.300	1154	704	572	347	343	239	080201	−0.50	0.03
51950.294	1452	784	701	485	403	277	100201	−0.51	0.03
51952.289	1135	825	559		286	191	120201	−0.59	0.03
52007.132	1481	1339	781	319	377		080401	−0.68	0.15
52008.129	938	843	401	296	168		090401	−0.71	0.13
52009.127	1091	1146	671	301	346		100401	−0.58	0.15
52010.124	1314	1257	898	470	299		110401	−0.62	0.14
52011.121	1359	1269	877	286	476		120401	−0.59	0.20
52012.119		1178	754	199	317		130401	−1.02	0.36
52013.116	1855	1313	592	382	204		140401	−0.90	0.11
52014.113	1403	1331	955	712	478		150401	−0.43	0.09
52015.110	1667	1090	743	552	289		160401	−0.67	0.09
52018.102	1212	785	528	371	213		190401	−0.68	0.07
52023.089	1841	606	502	370	161		240401	−0.87	0.14
52024.086		766	505				250401	−0.79	0.20
52025.083		564	458	214	170		260401	−0.81	0.10
52026.080	1232	1101	485	308	269		270401	−0.69	0.12
52027.078		645	653	332	266		280401	−0.62	0.15
52028.075		774	474	322	261		290401	−0.67	0.06
52030.069	942	516	382	262	171		010501	−0.66	0.04
52031.067	1033	887	402	321	187		020501	−0.70	0.12
52032.064	948	712	396	322	155		030501	−0.70	0.12
52033.061	940	772	520	336	233		040501	−0.57	0.08
52035.056	907	1303	647	343	427		060501	−0.45	0.19
52036.053	1908	956	776	695	406		070501	−0.56	0.09
52037.050	1216	928	684	515	321		080501	−0.51	0.07
52166.702	1270	722	540	375	310	400	140901	−0.42	0.09
52167.699		678	554	362	329	290	150901	−0.40	0.05

Table 3: *Flux density measurements of SS 433 (continued)*

(1)	(2)	(3)	(4)	(5)	(6)	(7)	(8)	(9)	(10)
52168.696	1200	764	568	399	344	480	160901	−0.36	0.10
52169.694	1090	754	533	361	266	300	170901	−0.47	0.06
52170.691	1230	598	542	368	276	160	180901	−0.62	0.05
52171.688	1080	763	544	350	295	200	190901	−0.56	0.02
52172.685	1090	626	539	388	337	190	200901	−0.52	0.04
52173.683	1260	738	581	370	344	210	210901	−0.56	0.02
52174.680	1100	724	484	362	261	180	220901	−0.59	0.02
52175.677	990	660	516	363	267	240	230901	−0.48	0.03
52176.675	1240	662	492	310	267	120	240901	−0.71	0.05
52177.672	1110	620	526	344	270	170	250901	−0.58	0.03
52179.666	1230	952	627	449	287	370	270901	−0.47	0.09
52180.664	1550	858	587	522	261	480	280901	−0.45	0.14
52181.661	1490	896	672	438	359	340	290901	−0.50	0.05
52182.658	1130	806	627	434	330	370	300901	−0.41	0.06
52183.655	1080	776	643	423	362	210	011001	−0.51	0.04
52184.653	1340	820	610	391	360	260	021001	−0.53	0.02
52185.650	1070	744	593	428	410	370	031001	−0.36	0.03
52186.647	1270	826	551	353	281		041001	−0.63	0.03
52188.642	1340	687	558	361	276		061001	−0.62	0.03
52189.639	1360	716	558	375	301		071001	−0.60	0.03
52190.636	1130	670	561	361	307		081001	−0.53	0.02
52191.634	1140	662	522	349	277		091001	−0.57	0.01
52192.631	1230	648	500	306	240		101001	−0.66	0.02
52193.628	1410	1000	578	318	261		111001	−0.73	0.07
52194.625	940	656	475	352	260		121001	−0.51	0.03
52195.623	1180	638	508	337	246		131001	−0.62	0.03
52196.620	1190	678	522	334			141001	−0.60	0.02
52197.617	1150	630	484	376	259		151001	−0.57	0.04
52198.615	1220	725	537	343	267		161001	−0.62	0.01
52199.612	1030	606	497	322	224		171001	−0.60	0.04
52200.609	1270	679	465	312	257		181001	−0.65	0.02
52201.606	1070	670	517	314	226		191001	−0.62	0.04
52202.604	1130	560	549				201001	−0.54	0.20
52203.601	1210	690	564	362	289		211001	−0.57	0.02
52204.598	1450	615	490	333	254		221001	−0.68	0.06
52205.595	1370	789	459	328	240		231001	−0.71	0.04
52206.593	1000	609	438	287	239		241001	−0.59	0.01
52207.590	1250	754	449	301	267		251001	−0.66	0.05
52208.587	1030	554	444	269	224		261001	−0.62	0.03
52209.584	980	679	458	261	240		271001	−0.61	0.05
52210.582	1010	659	466	310	195		281001	−0.65	0.06
52211.579	930	645	482	366			291001	−0.45	0.02
52212.576	1240	590	433	290	237		301001	−0.66	0.04
52213.574	760	627	437	314	236		311001	−0.48	0.05
52214.571	890	571	491	304	276		011101	−0.49	0.03
52215.568	1440	756	622	383	258		021101	−0.67	0.05
52216.565	1390	1300	669	489	336		031101	−0.60	0.11
52217.563	1610	990	663	398	320		041101	−0.67	0.03

Table 3: *Flux density measurements of SS 433 (continued)*

(1)	(2)	(3)	(4)	(5)	(6)	(7)	(8)	(9)	(10)
52218.560	1650	998	665	422	330		051101	−0.66	0.02
52219.557	2000	924	670	404	320		061101	−0.74	0.03
52221.552	1850	825	540	371	280		081101	−0.75	0.05
52222.549	1250	780	557	353	257		091101	−0.64	0.03
52223.546	1350	775	554	313	214		101101	−0.74	0.04
52224.544	1000	659	483	330	287		111101	−0.52	0.01
52225.541	1600	732	491	316	270		121101	−0.73	0.05
52226.538	840	635	499	328	274		131101	−0.47	0.04
52227.535	1100	723	564	328	267		141101	−0.59	0.04
52228.533	0900	726	519	389	276		151101	−0.47	0.06
52229.530	1000	680	463	320	271		161101	−0.55	0.02
52230.527	1200	712	486	290	199		171101	−0.73	0.04
52231.524	1300	632	438	248	218		181101	−0.74	0.04
52232.522	1100	622	436	296	188		191101	−0.69	0.04
52235.513	1190	822	540	366	268		221101	−0.61	0.04
52237.508	1160	843	467	287	287		241101	−0.63	0.08
52238.505	1450	892	502	292	219		251101	−0.79	0.05
52240.500	1330	576	548	373	282		271101	−0.59	0.08
52241.497	1450	533	482	284	174		281101	−0.80	0.09
52242.494	1100	702	446	300	204		291101	−0.68	0.04
52243.492	1100	588	407	312	234		301101	−0.61	0.04
52244.489	1100	544	427	285	225		011201	−0.63	0.03
52245.486	0800	492	470	221	164		021201	−0.64	0.09
52246.483	1500	605	361	230	187		031201	−0.85	0.06
52247.481	1250	384	407	282	158		041201	−0.73	0.14
52248.478	0950	504	260	240	147		051201	−0.73	0.09
52249.475	1500	497	356	212	193		061201	−0.83	0.10
52250.473	1350		303	303	172		071201	−0.79	0.15
52251.470	0810	519	367	278	192		081201	−0.57	0.04
52252.467	0790	561	400	262	186		091201	−0.59	0.05
52254.462		496	376	372	164		111201	−0.58	0.25
52255.459		371	402	269	267		121201	−0.26	0.10
52257.453	0700	410	541	331	215		141201	−0.41	0.12
52258.451	1200	656	486	364	257		151201	−0.60	0.03
52259.448	1520	685	508	380	252		161201	−0.69	0.06
52261.442	2300	823	488	355	253	150	181201	−0.84	0.06
52263.437	1350	863	694	423	337	410	201201	−0.44	0.08
52264.434	2200	1050	669	424	336	190	211201	−0.77	0.02
52265.432	2200	901	660	430	337	330	221201	−0.62	0.08
52266.429	1200	810	531	350	282	210	231201	−0.58	0.03
52268.423	950	633	493	354	289	250	251201	−0.45	0.02
52269.421	1150	659	490	364	365	470	261201	−0.32	0.10
52270.418	850	664	481	392	348	360	271201	−0.31	0.05
52273.410	960	530	417	277	285	240	301201	−0.45	0.06
52274.407	1100	641	470	354	322	160	311201	−0.57	0.05
52278.396	1300	1282	1247	883	604	210	040102	−0.54	0.17
52279.393	1520	2021	1798	1264	888	430	050102	−0.41	0.15
52280.391	2150	2071	1498	942	692	330	060102	−0.61	0.10

Table 3: *Flux density measurements of SS 433 (continued)*

(1)	(2)	(3)	(4)	(5)	(6)	(7)	(8)	(9)	(10)
52281.388	2210	2209	1791	1325	1046	370	070102	−0.53	0.14
52284.380	3150	2047	1313	854	633	560	100102	−0.60	0.05
52285.377	3010	1670	1112	696	515	340	110102	−0.71	0.01
52286.374	2600	1855	1154	777	624	370	120102	−0.63	0.03
52287.371	2500	1575	1003				130102	−0.64	0.09
52288.369	2510	1556	1105	676	492	410	140102	−0.62	0.04
52289.366	3000	2046	1519	1104	814	530	150102	−0.55	0.03
52290.363	2900	2286	1702	1073	752	370	160102	−0.66	0.08
52291.361	2800	1974	1551	1009	839	440	170102	−0.58	0.05
52292.358	2660	2108	1540	931	723	360	180102	−0.64	0.07
52293.355	2850	1933	1424	791	665	460	190102	−0.61	0.03
52294.352	2500	1462	948	583	452	210	200102	−0.78	0.04
52296.347	2150	1349	889	504	463	330	220102	−0.63	0.04
52297.344	2070	1196	884	528	411	210	230102	−0.72	0.04
52298.341	2350	1340	957	535	480	170	240102	−0.80	0.08
52299.339	2050	1224	825	491	359	240	250102	−0.71	0.02
52300.336	1880	1019	788	530	405	270	260102	−0.61	0.01
52301.333	1620	1004	778	449	347	400	270102	−0.51	0.08
52303.328	1600	0854	669	410	357	190	290102	−0.66	0.03
52304.325	1350	0944	665	448	379	240	300102	−0.56	0.02
52305.322	1800	0927	723	444	353	340	310102	−0.56	0.06
52306.320	1600	1021	698	464	384	260	010202	−0.59	0.01
52307.317	1300	857	692	441	366	260	020202	−0.52	0.02
52308.314	1550	794	747	592	308	170	030202	−0.66	0.09
52310.309	1200	803	576	319	258	140	050202	−0.70	0.04
52311.306	1500	788	538	397	304	420	060202	−0.46	0.11
52312.303	1150	768	557	369	281	100	070202	−0.74	0.10
52313.301	1220	692	536	361	320	290	080202	−0.48	0.05
52315.295	1200	668	561	342	293		100202	−0.57	0.03
52317.290	1280	750	491	370	252	140	120202	−0.69	0.04
52318.287	1000	751	529	340	299	220	130202	−0.51	0.03
52319.284	1320	743	528	372	301	300	140202	−0.50	0.06
52320.281	1000	628	462	362	327	230	150202	−0.46	0.02
52321.279	1230	605	473	339	262	210	160202	−0.56	0.04
52322.276	1100	575	476	268	277		170202	−0.59	0.06
52324.270	1040	659	510	373	299	140	190202	−0.60	0.06
52325.268	1300	713	509	292	229	220	200202	−0.61	0.06
52327.262	1370	620	456	309	279	220	220202	−0.58	0.06
52328.260	1300	515	445	253	283	160	230202	−0.62	0.07
52329.257	1250	553	445	253	249	160	240202	−0.64	0.05
52330.254	0900	658	471	286	288	210	250202	−0.49	0.04
52332.249	0850	664	470	306	267	280	270202	−0.41	0.06
52333.246	0880	565	433	241	216		280202	−0.60	0.04
52334.243	1100	554	415	241	295	160	010302	−0.59	0.06
52335.241	0890	495	416	347	247	150	020302	−0.53	0.05
52336.238	1500	495	454	290	275	170	030302	−0.64	0.08
52337.238	1600	696	502	342	291	180	040302	−0.67	0.04
52370.145		664	436	285	251	122	060402	−0.71	0.06

Table 3: *Flux density measurements of SS 433 (continued)*

(1)	(2)	(3)	(4)	(5)	(6)	(7)	(8)	(9)	(10)
52371.142		589	276	292	221	166	070402	−0.49	0.12
52372.139		564	423	294	246	110	080402	−0.69	0.09
52373.137		489	436	269	249	170	090402	−0.49	0.04
52374.134		679	415	287	236	165	100402	−0.61	0.04
52375.131		570	389	290	215	172	110402	−0.54	0.04
52376.128		612	450	281	231	193	120402	−0.54	0.05
52377.126		545	428	296	219	192	130402	−0.49	0.05
52378.123		535	460	298	219	119	140402	−0.68	0.07
52379.120		529	414	306	229	225	150402	−0.41	0.06
52380.118		699	435	314	221	99	160402	−0.83	0.08
52381.115		581	455	269	229	134	170402	−0.66	0.04
52382.112		564	379	270	214	154	180402	−0.57	0.03
52383.109		618	443	271	198	220	190402	−0.51	0.11
52384.107		593	420	295	234	198	200402	−0.50	0.05
52385.104		666	432	316	263	150	210402	−0.63	0.05
52386.101		596	408	250	231	110	220402	−0.72	0.06
52387.098		544	380	255	200	125	230402	−0.65	0.01
52388.096		540	371	244	174	154	240402	−0.58	0.07
52389.093		436	376	268	218	175	250402	−0.43	0.03
52390.090		543	381	237	201	180	260402	−0.51	0.07
52391.087		491	356	207	201	184	270402	−0.46	0.09
52392.085		440	360	228	186	135	280402	−0.55	0.03
52393.082		550	326	236	173	195	290402	−0.48	0.12
52395.077		900	503	267	296		010502	−0.75	0.17
52396.074		572	426	289	292		020502	−0.45	0.08
52397.071		648	438	279	302		030502	−0.52	0.12
52398.068		1021	460	326	261		040502	−0.82	0.16
52399.066		958	427	327	293		050502	−0.71	0.19
52400.063		802	479	354	230		060502	−0.74	0.09
52401.060		731	515	339	331		070502	−0.52	0.08
52402.057		1073	597	374	177		080502	−1.06	0.15
52403.055			616	472	295		090502	−0.66	0.22
52404.052		793	661	479	354		100502	−0.50	0.06
52405.049		700	610	392	342		110502	−0.48	0.05
52406.047		767	487	362	151		120502	−0.92	0.22
52407.044		791	530	444	277		130502	−0.60	0.11
52408.041		657	629	442	387		140502	−0.36	0.06
52409.038		855	718	475	389		150502	−0.51	0.04
52410.036		792	738	522	496		160502	−0.33	0.05
52411.033		1073	714	453	388		170502	−0.65	0.05
52412.030		1138	626	395	246		180502	−0.92	0.08
52413.027		1156	621	391	394		190502	−0.69	0.15
52414.025		909	603	413	346		200502	−0.61	0.04
52415.022		827	596	413	377		210502	−0.51	0.05
52416.019		943	571	414	205		220502	−0.88	0.16
52551.690		920	607	520	327		041002	−0.58	0.12
52552.687		1350	977	606	483		051002	−0.66	0.01
52553.684		1100	756	475	320		061002	−0.76	0.05

Table 3: *Flux density measurements of SS 433 (continued)*

(1)	(2)	(3)	(4)	(5)	(6)	(7)	(8)	(9)	(10)
52554.681		1000	668	387	279		071002	−0.81	0.01
52555.679		950	553	423	290		081002	−0.70	0.09
52556.676		1100	587	393	312		091002	−0.77	0.10
52557.673		1100	702	449	367		101002	−0.69	0.04
52558.670		1080	848	501	349		111002	−0.72	0.07
52559.668		1030	734	437	399		121002	−0.63	0.06
52560.665		1140	682	404	282		131002	−0.87	0.03
52561.662		890	777	469			141002	−0.54	0.14
52562.660		875	623	416	361		151002	−0.57	0.03
52563.657		1200	605	431	365		161002	−0.72	0.14
52564.654		970	614	385	307		171002	−0.72	0.04
52565.651		1050	587	392	278		181002	−0.80	0.07
52566.649		1150	644	442	276		191002	−0.85	0.09
52567.646		510	581		258		201002	−0.48	0.25
52569.640		800	581	362	261		221002	−0.70	0.03
52570.638		870	532	364	225		231002	−0.81	0.08
52571.635		920	635	365	272		241002	−0.78	0.02
52572.632		1020	516	411	326		251002	−0.67	0.14
52573.629		1050	553	340	188		261002	−1.03	0.10
52574.585		830	551	333	291		271002	−0.68	0.05
52575.582		850	549	359	213		281002	−0.83	0.09
52576.580		740	565	410	250		291002	−0.64	0.11
52577.577		850	504	391	287		301002	−0.64	0.09
52578.574		900	614	430	310		311002	−0.65	0.04
52579.571		885	629	387	306		011102	−0.68	0.01
52580.569		715	635	363	297		021102	−0.59	0.09
52581.566		1300	638	420	290		031102	−0.90	0.10
52583.561		800	591	360	305		051102	−0.63	0.03
52584.558		930	548	344	304		061102	−0.71	0.09
52585.555		730	565	378	220		071102	−0.72	0.12
52586.552		1020	502	312	327		081102	−0.73	0.19
52587.550		770	562	329	224		091102	−0.78	0.05
52588.547		1050	460	371	247		101102	−0.83	0.17
52589.544		850	520	342	141		111102	−1.04	0.21
52590.541		750	489	297	299		121102	−0.61	0.11
52591.539		880	559	380	260		131102	−0.74	0.05
52592.536		850	545	363	301		141102	−0.65	0.05
52593.533		1000	565	299	336		151102	−0.74	0.18
52594.530		1090	623	344	379		161102	−0.71	0.17
52595.528		880	602	383	212		171102	−0.85	0.12
52596.525		900	570	369	174		181102	−0.96	0.16
52597.522		830	537	352	336		191102	−0.59	0.09
52598.520		810	550	339	244		201102	−0.75	0.02
52599.517		775	502	365	215		211102	−0.75	0.11
52600.514		710	452	322	221		221102	−0.70	0.06
52601.511		849	511	389	283		231102	−0.65	0.08
52602.509		1019	554	431	349		241102	−0.64	0.12
52608.492		731	633	336	241	162	301102	−0.72	0.06

Table 3: *Flux density measurements of SS 433 (continued)*

(1)	(2)	(3)	(4)	(5)	(6)	(7)	(8)	(9)	(10)
52609.490		792	663	384	290	257	011202	−0.55	0.07
52611.484		811	568	327	276	127	031202	−0.80	0.06
52612.481		714	543	317	241	180	041202	−0.64	0.04
52613.479		738	542	319	254	141	051202	−0.74	0.03
52615.473		697	592		320	197	071202	−0.57	0.05
52616.470		748	653	414	304	254	081202	−0.52	0.05
52618.465		815	573	267	295	141	101202	−0.76	0.09
52619.462		759	544	367	301	302	111202	−0.44	0.08
52620.459		743	594	417	315	208	121202	−0.57	0.03
52621.457		766	605	354	287	143	131202	−0.74	0.06
52622.454		767	684	413	340	178	141202	−0.66	0.08
52623.451		916	617	451	331	293	151202	−0.52	0.06
52625.446		826	630	381	314	165	171202	−0.71	0.05
52626.443		762	582	356	323	303	181202	−0.44	0.08
52627.440		747	587	369	273	169	191202	−0.67	0.03
52628.438		745	546	441	322	197	201202	−0.57	0.05
52629.435		693	555	343	260	299	211202	−0.44	0.11
52630.433		725	555	360	260	228	221202	−0.55	0.06
52635.419		751	546	391	281	177	271202	−0.64	0.03
52636.416		758	541	374	300	146	281202	−0.70	0.07
52637.413		711	540	333	297	195	291202	−0.58	0.03
52639.408		680	584	369	293	293	311202	−0.43	0.08
52641.402		747	526	384	267	388	020103	−0.35	0.15
52642.399		592	542	360	296	461	030103	−0.20	0.15
52643.397		726	531	287	310	162	040103	−0.65	0.08
52644.394		721	579	389	302	191	050103	−0.60	0.03
52645.391		607	557	324	283	298	060103	−0.38	0.10
52646.388		691	536	323	298	317	070103	−0.39	0.10
52647.386		753	463	355	364	131	080103	−0.68	0.14
52648.383		683	527	296	263	215	090103	−0.55	0.06
52649.380		669	498	323	254	162	100103	−0.63	0.01
52650.378		737	564	348	304	261	110103	−0.49	0.06
52651.375		692	560	331	305	217	120103	−0.53	0.04
52653.369		716	617	363	321	229	140103	−0.53	0.04
52654.367		757	585	339	283	240	150103	−0.55	0.06
52655.364		773	580	383	304	110	160103	−0.82	0.13
52656.361		710	574	361	269	258	170103	−0.50	0.07
52657.358		787	594	346	294	176	180103	−0.67	0.03
52658.356		780	565	295	259	224	190103	−0.59	0.09
52660.350		670	498	283	253	238	210103	−0.50	0.09
52661.348		604	492	272	250	200	220103	−0.52	0.06
52663.342		643	542	332	243	138	240103	−0.70	0.06
52664.339		801	597	336	283	236	250103	−0.58	0.07
52667.331		627	479	269	217	219	280103	−0.52	0.10
52668.328		689	498	289	203	94	290103	−0.88	0.06
52669.326		619	535	304	267	145	300103	−0.65	0.06
52670.323		697	529	316	231	218	310103	−0.57	0.08
52671.320		709	548	274	213	228	010203	−0.58	0.13

Table 3: *Flux density measurements of SS 433 (continued)*

(1)	(2)	(3)	(4)	(5)	(6)	(7)	(8)	(9)	(10)
52672.318		646	571	318	230	280	020203	−0.46	0.13
52674.312		659	539	289	235		040203	−0.69	0.08
52675.309		763	579	348	298	172	050203	−0.66	0.03
52676.307		780	509	318	280	320	060203	−0.43	0.13
52677.304		635	570	354	259	145	070203	−0.68	0.07
52678.301		655	492	273	226	143	080203	−0.69	0.03
52681.293		778	551	325	244	307	110203	−0.48	0.14
52682.290		723	522	302	262	202	120203	−0.59	0.05
52683.287		826	544	279	246	305	130203	−0.50	0.17
52684.285		674	501	279	252	168	140203	−0.63	0.04
52685.282		538	500	299	223	205	150203	−0.49	0.08
52686.279		561	534	279	211	188	160203	−0.56	0.09
52688.273		716	582	311	290	188	180203	−0.61	0.05
52689.270		649	578	327	247	85	190203	−0.89	0.15
52690.267		675	532	309	255	129	200203	−0.73	0.06
52691.264		710	496	279	235	144	210203	−0.71	0.03
52692.261		644	504	320	219	389	220203	−0.32	0.20
52693.258		812	542	328	238	243	230203	−0.58	0.10
52714.203		760	425	358	293		160303	−0.56	0.12
52715.200		865	735	403	266		170303	−0.76	0.11
52716.197		785	621	374	229	364	180303	−0.45	0.19
52717.195		631	547	437	345	200	190303	−0.50	0.08
52718.192		761	547	341	298	237	200303	−0.53	0.05
52719.189		575	526	382	283	389	210303	−0.25	0.12
52721.184		741	497	317	325	379	230303	−0.32	0.14
52722.181		1013	627	453	349	347	240303	−0.49	0.09
52723.178		937	717	490	423	264	250303	−0.55	0.03
52724.176		1302	736	519	311	233	260303	−0.77	0.07
52727.168		1042	619	480	284	155	290303	−0.82	0.08
52728.165		789		421	418	325	300303	−0.39	0.05
52729.162		707	644	484	298	339	310303	−0.40	0.10
52730.159		654	629	457	273	293	010403	−0.43	0.11
52731.156		365	588	386	276	382	020403	−0.11	0.17
52732.154		843	615	411	361	254	030403	−0.53	0.02
52733.151		825	525	397	375	245	040403	−0.50	0.05
52734.148		781	561	395	331	634	050403	−0.17	0.21
52736.143		992	751	548	495	296	070403	−0.51	0.04
52737.140		1123	718	498	419	237	080403	−0.66	0.04
52738.137		1101	647	533	424	427	090403	−0.41	0.10
52739.135		873	657	437	377	464	100403	−0.33	0.12
52740.132		873	681	467	428	332	110403	−0.44	0.03
52741.129		836	671	462	420	417	120403	−0.34	0.07
52742.126		1079	761	498	370	278	130403	−0.62	0.03
52743.124		1186	699	519	480	361	140403	−0.50	0.07
52744.121		879	696	517	499	451	150403	−0.30	0.05
52745.118		1037	728	503	447	394	160403	−0.44	0.06
52746.115		876	741	461	436	359	170403	−0.42	0.05
52747.113		1199	633	423	387	251	180403	−0.66	0.08

Table 3: *Flux density measurements of SS 433 (continued)*

(1)	(2)	(3)	(4)	(5)	(6)	(7)	(8)	(9)	(10)
52748.110		1045	548	492	420	485	190403	−0.32	0.14
52749.107		941	717	532	391	465	200403	−0.36	0.10
52750.105		1022	720	507	447	387	210403	−0.44	0.05
52751.102		1269	700	444	331		220403	−0.82	0.07
52752.099		1219	762	501	328		230403	−0.79	0.06
52753.096		1012	570	535	423	262	240403	−0.54	0.09
52754.094		1043	715	406	307	546	250403	−0.38	0.22
52756.088		948	609	484	362	353	270403	−0.44	0.08
52758.083		999	487	482	378		290403	−0.53	0.19
52760.077		1009	595	461	360	212	010503	−0.65	0.05
52761.075		877	663	435	374	559	020503	−0.26	0.16
52762.072		962	752	488	377	455	030503	−0.39	0.12
52763.069		1075	787	438	342		040503	−0.74	0.04
52764.067		971	612	430	358	219	050503	−0.63	0.04
52765.065		950	657	495	380	383	060503	−0.42	0.08
52766.063		1044	657	444	297	253	070503	−0.65	0.07
52767.060		1069	709	481	371	319	080503	−0.55	0.06
52768.097		964	557	441	403		090503	−0.53	0.12
52769.094		957	576	418	360	278	100503	−0.53	0.06
52770.092		1125	578	388	259	220	110503	−0.73	0.10
52771.089		907	648	493	335	376	120503	−0.43	0.10
52772.086			746	484	399	263	130503	−0.60	0.01
52773.083		1228	762	500	489	211	140503	−0.72	0.09
52774.081		1137	870	528	423	339	150503	−0.57	0.05
52776.075		1307	769	511	447	554	170503	−0.41	0.16
52777.072		972	723	475	433	471	180503	−0.35	0.10
52778.070		1286	697	482	447		190503	−0.66	0.13
52779.067		975	790	511	455		200503	−0.51	0.04
52780.063		943	639	448	362	299	210503	−0.52	0.05
52781.060		1000	635	535	431	481	220503	−0.33	0.10
52782.057		1000	635	535	431		230503	−0.49	0.09
52783.054		1071	622	490	468	132	240503	−0.81	0.19
52784.051		1003	517	470	386		250503	−0.54	0.16
52785.048		962	641	434	397	414	260503	−0.39	0.10
52786.045		1067	659	380	321	269	270503	−0.63	0.09
52788.001		915	561	396	275	372	290503	−0.45	0.16
52788.998		1127	489	387	306	313	300503	−0.45	0.16
52789.995		1040	467	424	339	531	310503	−0.29	0.22
52790.993		963	579	458	273	589	010603	−0.30	0.25
52791.990		1180	526	368	376	288	020603	−0.57	0.14
52793.984		1034	540	307	400		040603	−0.66	0.24
52794.982		1007	598	451	376	502	050603	−0.33	0.16
52795.979		972	601	461	349	413	060603	−0.40	0.12
52796.976		940	612	429	415	287	070603	−0.50	0.05
52797.974		874	614	423	371	391	080603	−0.38	0.09
52798.971		1000	516	417	304	207	090603	−0.66	0.08
52799.968		1066	517	342	380	189	100603	−0.69	0.12
52800.965		1238	550	375	337		110603	−0.80	0.18

Table 3: *Flux density measurements of SS 433 (continued)*

(1)	(2)	(3)	(4)	(5)	(6)	(7)	(8)	(9)	(10)
52801.962		1006	602	360	257		120603	−0.85	0.03
52802.959		756	585	352	397		130603	−0.47	0.12
52803.956		685	533	439	326		140603	−0.44	0.06
52804.953		791	535	363	344		150603	−0.54	0.08
52805.950		665	476	366	313		160603	−0.47	0.04
52806.947		1264	508	345	340	485	170603	−0.42	0.25
52807.944		795	663	406	373	354	180603	−0.40	0.08
52808.941		718	663	422	364		190603	−0.46	0.07
52809.938		718	663	422	364		200603	−0.46	0.07
52811.932		980	505	402	341		220603	−0.63	0.14
52815.920		917	629	445	365		260603	−0.57	0.03
52817.914		1014	605	419	323		280603	−0.70	0.06
52819.908		1065	578	361	351		300603	−0.71	0.14
52876.799		1543		393			250803	−1.13	2.69
52877.797		1165	619	415	345		260803	−0.75	0.11
52878.794		1017	590	330	335		270803	−0.74	0.14
52879.791		956	644	426	291		280803	−0.73	0.05
52880.789		1990	644	403	282		290803	−1.33	0.31
52881.786		978	616	337	379		300803	−0.66	0.16
52882.783		986	611	458	291		310803	−0.71	0.09
52883.780		1088	593	325	279		010903	−0.87	0.09
52884.778		1101	573	400	261		020903	−0.85	0.10
52885.775		685	597	357	249		030903	−0.65	0.10
52886.772		978	582	390	312		040903	−0.71	0.06
52888.767		1024	626	413	322		060903	−0.72	0.05
52889.764		1446	644	350	315		070903	−0.97	0.16
52890.761		995	618	291	276		080903	−0.86	0.11
52891.759		785	487	316	349		090903	−0.54	0.15
52892.756		833	522	323	338		100903	−0.60	0.13
52893.756		883	616	452	333		110903	−0.59	0.04
52894.750		731	651	421	388		120903	−0.44	0.06
52895.748		959	557	335	298		130903	−0.75	0.09
52896.745		621	579	298	377		140903	−0.43	0.18
52897.742			583	326	302		150903	−0.65	0.17
52898.739		880	694	426	373		160903	−0.57	0.05
52899.737		1074	723	522	383		170903	−0.62	0.04
52900.734		1187	825	454	254		180903	−0.95	0.11
52901.731		845	595	367	306		190903	−0.65	0.03
52902.728		1307	460	349	302		200903	−0.86	0.26
52903.726		851	580	335	307		210903	−0.67	0.07
52904.723		735	617	393	330		220903	−0.53	0.05
52949.553		723		373	351	268	061103	−0.44	0.05
52950.556		675		334	275	292	071103	−0.41	0.12
52951.553				310	243	248	081103	−0.19	0.18
52955.542		732	522	347	311	156	121103	−0.68	0.07
52957.537		673	508	335	286	221	141103	−0.52	0.05
52959.531		780	428	332	286	245	161103	−0.52	0.08
52961.526		766	508	340	312	269	181103	−0.49	0.07

Table 3: *Flux density measurements of SS 433 (continued)*

(1)	(2)	(3)	(4)	(5)	(6)	(7)	(8)	(9)	(10)
52963.520		641		273	295	145	201103	−0.63	0.11
52967.509		735	473	365	292	191	241103	−0.60	0.01
52971.498		787	498	356	312	123	281103	−0.79	0.11
52973.493		669	468	345	266	202	301103	−0.55	0.03
52975.487		682	422	293	221	216	021203	−0.55	0.09
52977.482		668	405	323	282	245	041203	−0.45	0.06
52979.477		750	478	363	303	176	061203	−0.63	0.03
52985.460		746	354	307	258	268	121203	−0.46	0.14
52987.455		700	365	274	239	204	141203	−0.55	0.09
52989.449		622	418	333	281	176	161203	−0.55	0.03
52991.444		716	417	330	279	255	181203	−0.47	0.08
52993.438		679	336	273	239	179	201203	−0.58	0.08
52997.427		726	393	284	230	197	241203	−0.60	0.08
52999.422		704	383	285	191	219	261203	−0.57	0.14
53001.417		632	421	271	266	146	281203	−0.64	0.06
53003.411		676	443	331	238	145	301203	−0.69	0.04
53007.400		664	440	288	242	90	030104	−0.86	0.12
53017.373		1084	667	413	318	267	130104	−0.66	0.08
53019.367		1143	811	527	414	278	150104	−0.65	0.04
53020.365		1143	680	552	452	259	160104	−0.64	0.04
53022.359		1090	587	420	331	282	180104	−0.62	0.08
53023.356		958	523	388	334	311	190104	−0.51	0.10
53024.353		932	472	443	275	285	200104	−0.55	0.12
53025.350		981	485	437	321	301	210104	−0.53	0.10
53026.347		931	460	423	313	207	220104	−0.65	0.06
53027.344		807	481	396	328	231	230104	−0.55	0.03
53028.341		880	438	420	284	374	240104	−0.41	0.16
53029.338		836	461		233	294	250104	−0.51	0.18
53031.332		705	397	353	269	235	270104	−0.49	0.07
53032.332		793	412	365	284	190	280104	−0.62	0.05
53033.329		866	472	383	313	183	290104	−0.67	0.04
53034.323		847	458	422	342	275	300104	−0.49	0.07
53035.320		802	439	402	312	225	310104	−0.55	0.05